8-3-2010

Programmable Periodicity of Quantum Dot Arrays with DNA Origami Nanotubes

Hieu Bui
Boise State University

Craig Onodera
Boise State University

Carson Kidwell
Boise State University

YerPeng Tan
Boise State University

Elton Graugnard
Boise State University

See next page for additional authors

NANO LETTERS

pubs.acs.org/NanoLett

Programmable Periodicity of Quantum Dot Arrays with DNA Origami Nanotubes

Hieu Bui,[†] Craig Onodera,[‡] Carson Kidwell,[‡] YerPeng Tan,[‡] Elton Graugnard,[‡] Wan Kuang,[†] Jeunghoon Lee,[§] William B. Knowlton,[†,‡] Bernard Yurke,[†,‡] and William L. Hughes*[,‡]

[†]Department of Electrical and Computer Engineering, [‡]Department of Materials Science and Engineering, and [§]Department of Chemistry and Biochemistry, Boise State University, Boise Idaho 83725

ABSTRACT To fabricate quantum dot arrays with programmable periodicity, functionalized DNA origami nanotubes were developed. Selected DNA staple strands were biotin-labeled to form periodic binding sites for streptavidin-conjugated quantum dots. Successful formation of arrays with periods of 43 and 71 nm demonstrates precise, programmable, large-scale nanoparticle patterning; however, limitations in array periodicity were also observed. Statistical analysis of AFM images revealed evidence for steric hindrance or site bridging that limited the minimum array periodicity.

KEYWORDS DNA, origami, nanoparticles, quantum dot, self-assembly, periodic

The ability to precisely pattern nanoparticles is essential for realizing the potential of nanoelectronic and nanoplasmonic devices.[1−3] Over the past decade, DNA oligonucleotides have been programmed to aggregate,[4,5] crystallize,[6,7] and self-assemble into spatially discrete assemblies[8−13] and linear arrays.[14−16] DNA nanotechnology offers a compelling approach toward programmable nanoparticle patterning.[17−20] By implementing basic design rules, DNA can be used to form complex nanostructures using the methods of either tiled DNA motifs or DNA origami.[21−27] When functionalized, these nanostructures can serve as two-dimensional[28−36] and three-dimensional[37] nanoparticle scaffolds. Several groups have reported successful attachment of semiconductor quantum dots (QDs) to functionalized DNA.[10,33,38] Sharma et al. recently reported the fabrication of periodic QD arrays formed by tiling DNA motifs.[33] While tiling methods have the ability to create highly ordered complex arrays, they tend to create continuous sheets; the boundaries of which are not well controlled.

Presented here is a method of fabricating nanoparticle arrays with controlled periodicity using three-dimensional, six-helix DNA origami nanotubes. DNA origami nanotubes of predetermined dimensions were used to precisely arrange nanoparticles by incorporating binding sites along the axis of the nanotube using biotin-labeled staple strands. The unique sequence of each staple strand permits precise spatial control and modular design of periodic or aperiodic binding sites. The three-dimensional DNA origami nanotubes provide a rigid structure for nanoparticle attachment in solution. Additionally, the extension of the DNA nanotubes into networks via dimerization, polymerization, or branching offers controlled fabrication of more complex nanoparticle structures.

The DNA origami nanotubes used in this research were designed using the principles reported by Mathieu et al.[39] and Douglas et al.[40] where the single-stranded M13mp18 DNA molecule was folded into a six-helix nanotube bundle using the DNA origami method developed by Rothemund.[25] The design reported here uses 170 unique staple strands to fold the single-stranded M13mp18 scaffold, resulting in DNA nanotubes with blunt ends that do not dimerize. The nanotube design is illustrated and described in detail in the Supporting Information S1. Staple strands include 9 strands with 69 nucleotides, 9 strands with 35 nucleotides, and 152 strands with 42 nucleotides (see Supporting Information S2). The DNA nanotubes were designed to be 412 nm in length and 6 nm in diameter. To incorporate nanoparticle binding sites, prior to nanotube synthesis, selected staple strands were extended with a 2.2 nm tether consisting of 5 thymine nucleotides and modified with biotin at the 3′ end. The resulting DNA nanotubes possessed precisely spaced biotin binding sites for controlled positioning of streptavidin-conjugated nanoparticles along the length of the nanotube (see Supporting Information S3).

To test controlled nanoparticle patterning, four distinct DNA nanotubes were synthesized with evenly spaced binding sites designed to attach 5, 9, 15, or 29 streptavidin-conjugated nanoparticles to form arrays with periodicities of 71, 43, 29, or 14 nm, respectively. The biotin-labeled DNA nanotubes were designed by functionalizing the appropriate staple strands, as described above. The nanotubes were synthesized by combining M13mp18 viral DNA (New England Biolabs) with unmodified and biotin-labeled staple strands (Integrated DNA Technologies) in a molar ratio of 1:10:10 in a solution of 1 × TAE, Mg^{2+} (40 mM tris, 20 mM acetic acid, 2 mM ethylenediaminetetracetic acid (EDTA),

* To whom correspondence should be addressed: WillHughes@BoiseState.edu.
Received for review: 03/27/2010
Published on Web: 08/03/2010

DOI: 10.1021/nl101079u | *Nano Lett.* **2010,** *10,* 3367–3372

and 12.5 mM magnesium acetate; pH 8.0). TAE, magnesium acetate tetrahydrate, and laboratory grade water (Milli-Q Water, Millipore) were purchased from Sigma Aldrich. All DNA strands were used without further purification. To form nanotubes, the DNA solution was thermally annealed at 90 °C for 20 min, then cooled to 20 °C at ~1 °C per minute using a thermal cycler (Mastercycler, Eppendorf). After the nanotubes were synthesized, the solution was centrifuged using a centrifugal filter (100 000 molecular weight cut off) at 500 g for 15 min to remove excess staple strands and small, unbound DNA fragments.

Successful formation of biotin-labeled DNA nanotubes was confirmed via atomic force microscopy (AFM). During sample preparation, 5 μL of DNA nanotube solution was dispersed onto freshly cleaved V-4 grade mica with 20 μL of 1 × TAE, Mg^{2+} buffer and allowed to adsorb onto the surface for 5 min. Then, the surface was washed with Milli-Q water and dried with compressed air. Imaging of functionalized nanotubes was performed using AFM (Multimode Picoforce with a Nanoscope IV controller, Veeco Metrology) under ambient conditions in AC mode using silicon cantilever-based tips (PPP-NCH, Nanosensors). Cantilevers had a nominal spring constant of 42 N/m with a range of 10−130 N/m. To validate the linearity, stability, and accuracy of the piezoelectric scanner, the AFM was calibrated using (1) a surface topography reference (STR) with precision fabricated silicon dioxide rectangular features (VLSI Standards), and (2) the atomic step height of freshly cleaved, ZYH grade, highly ordered pyrolytic graphite (HOPG, Veeco Metrology) (see Supporting Information S4).

Figure 1 shows DNA origami nanotubes with nine biotin binding sites as synthesized (a−e), after functionalization with streptavidin (f−j), and after functionalization with streptavidin-conjugated quantum dots (k−o). Figure 1a illustrates the biotin-labeled nanotube structure, while panels b and c show low- and high-magnification AFM height images, respectively. The dashed line in panel c indicates the location of the cross-sectional height profile in panel d. From this profile, a nanotube height of ~2.6 nm is measured. When measured under various imaging conditions, the mean nanotube height ranged from 3.5 ± 0.1 to 1.7 ± 0.4 nm (see Supporting Information S5). The axial profile shown in panel e emphasizes relative height variations along the nanotube length (see Supporting Information S6). The mean nanotube length was measured to be 436 ± 14 nm from 100 samples and was independent of the imaging conditions. The DNA origami nanotubes were designed to have a circular cross-section equivalent to 3 double helices (i.e., 6 nm)[39] with an expected length of 412 nm. While the nanotube length is in agreement with the expected value, the height is less than the expected diameter. According to Douglas et al., the diameter of DNA nanotubes with six helices was ~7 ± 2 nm using transmission electron microscopy (TEM).[40] Sources of deviation may include the nanotube collapsing onto the mica surface because of surface van der Waals forces,[41,42] capillary effects encountered when imaging in ambient conditions,[41] and compressive forces during AFM imaging[43−45] (see Supporting Information S5). For example, reduced AFM height profiles for soft biological samples have been reported in multiple studies.[41,46,47]

Once biotin-labeled DNA nanotubes were verified via AFM, the accessibility and reactivity of the biotin attachment sites were tested by combining a 1 nM solution of biotin-labeled nanotubes with pure, lyophilized streptavidin purchased from Sigma Aldrich that was resuspended in Milli-Q water at 200 nM. The components were allowed to react for 2 h at room temperature. The reacted nanotubes were dispersed onto a freshly cleaved mica surface and dried as described above. Figure 1f illustrates the biotin-labeled DNA nanotubes with attached streptavidin. The successful attachment of nine streptavidin molecules is clearly observed by comparison of the high-magnification AFM images without streptavidin in panel c and with streptavidin in panel h. The cross-sectional profile in panel i, obtained at an apparent streptavidin site, reveals a height increase of ~0.5 nm relative to the nanotube shown in panel d. The axial profile in panel j clearly displays nine peaks with a periodicity of 45 nm, very close to the expected value of 43 nm.

While the measured height increase at a streptavidin site was ~0.5 nm, the mean height of free streptavidin, dispersed onto freshly cleaved mica, was measured to range from 2.3 ± 0.5 to 0.7 ± 0.2 nm under various imaging conditions (see Supporting Information S5). Although X-ray analysis of dehydrated streptavidin crystals indicated a thickness of 4.6 nm,[48−51] Weisenhorn et al. imaged streptavidin under different AFM contact forces and demonstrated that the maximum height varied between 1.12, 0.65, and 0.25 nm at 30, 60, and 150 pN, respectively.[44] Thus, the streptavidin heights measured here are consistent with previous studies.

CdSe/ZnS core/shell streptavidin-conjugated quantum dots (Qdot 585, Invitrogen), hereafter referred to as quantum dots, with an average diameter of 15−20 nm were chosen to test nanoparticle attachment. To ensure a high attachment yield, a 1 nM solution of functionalized DNA nanotubes was combined at room temperature with a 200 nM solution of quantum dots for 2 h. The reacted DNA nanotubes with attached quantum dots were dispersed onto a mica surface and dried as described above. Figure 1k illustrates the attachment of the quantum dots to the biotin-labeled DNA nanotubes. Figure 1l,m respectively shows low- and high-magnification AFM height images of the DNA nanotubes with attached quantum dots. When compared to panels c and h, quantum dots attach to biotin-labeled DNA nanotubes with the same periodic spacing. Additionally, the cross-sectional profile across an apparent quantum dot in panel n yields a height of 5.5 nm, nearly twice the measured height of the nanotube with no attached particles. The mean height of free quantum dots, dispersed onto freshly cleaved mica, was measured to range from 5.5 ± 0.6 to 4.7 ± 0.7 nm

DOI: 10.1021/nl101079u | Nano Lett. 2010, 10, 3367–3372

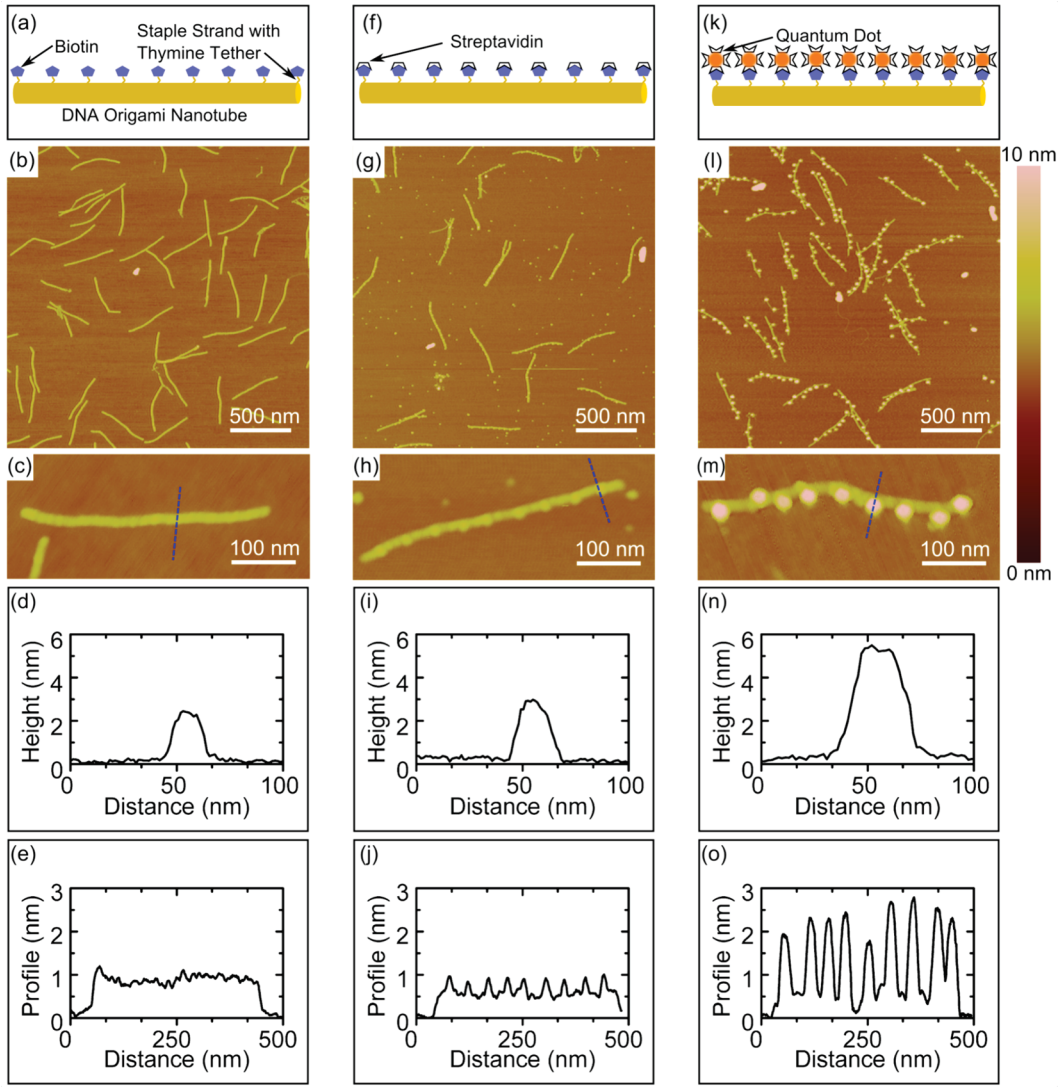

FIGURE 1. Schematics, AFM images at low magnification (upper) and high magnification (lower), and cross-sectional (upper) and axial (lower) height profiles of functionalized DNA origami nanotubes with nine biotin binding sites with (a−e) no attached nanoparticles; (f−j) attached streptavidin; and (k−o) attached streptavidin-conjugated quantum dots. The dashed lines in the high-magnification AFM images indicate the location of the cross-sectional profiles. Axial profiles represent the average of multiple profiles across the width of the nanotube (see Supporting Information S6).

under various imaging conditions (see Supporting Information S5). Although the diameter of the streptavidin-conjugated quantum dots is ∼20 nm in solution according to manufacturer specifications, the AFM height measurements of the dehydrated quantum dots correspond to the approximate diameter of the CdSe/ZnS quantum dot core/shell, as measured by TEM (see Supporting Information S7). Thus, with the chosen AFM imaging conditions the dehydrated streptavidin and polymer layer contributed very little to the measured height of the conjugated nanoparticle. The axial profile in panel o again shows nine equally spaced peaks with a periodicity of 49 nm.

To illustrate the flexibility of the design and confirm control over nanoparticle attachment, functionalized DNA nanotubes were synthesized with 5, 9, 15, and 29 biotin attachment sites to enable the formation of quantum dot arrays with periodicities of 71, 43, 29, and 14 nm, respectively. These nanotubes were reacted with quantum dots and dispersed onto mica substrates as in the manner described above. Figure 2 shows high-magnification height images of quantum dots attached to DNA nanotubes with (a) 5, (b) 9, (c) 15, and (d) 29 biotin binding sites. Successful attachment to each biotin binding site was observed for nanotubes with 5 or 9 available sites; however, attached quantum dots were not observed at each site for nanotubes with 15 or 29 available sites. The average quantum dot spacings were measured to be approximately 71 ± 3, 49 ± 4, 46 ± 5, and 31 ± 4 nm for nanotubes with 5, 9, 15, and 29 available biotin binding sites, respectively. The measured spacings for 5 and 9 binding sites agree well with the predicted periods of 71 and 43 nm. However, the arrays seen in Figure 2c,d formed with a reduced number of quantum dots and,

DOI: 10.1021/nl101079u | *Nano Lett.* **2010,** *10,* 3367–3372

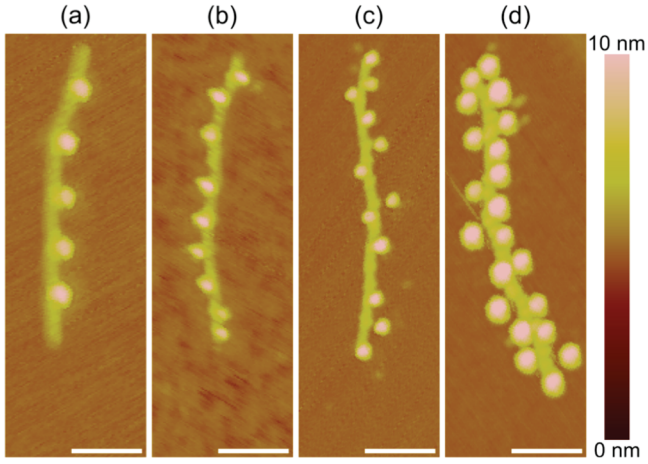

FIGURE 2. High-magnification AFM images of streptavidin-conjugated quantum dots attached to functionalized DNA origami nanotubes with (a) 5 binding sites, 71 nm period; (b) 9 binding sites, 43 nm period; (c) 15 binding sites, 29 nm period; and (d) 29 binding sites, 14 nm period. All scale bars are 100 nm. Note (c) and (d) have fewer attached quantum dots than available binding sites. In addition, the diameter of quantum dots varies between images because of variation in tip radii between scans.

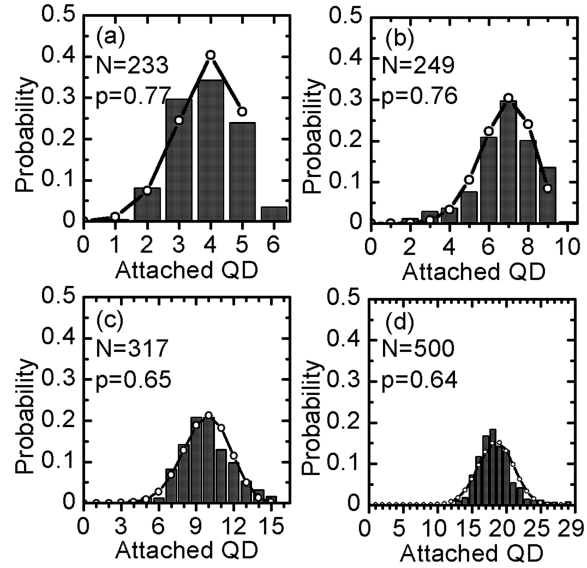

FIGURE 3. Histograms (bars) and calculated binomial distributions (lines) for the number of attached quantum dots for DNA nanotubes with (a) 5, (b) 9, (c) 15, and (d) 29 biotin binding sites. Data for each histogram were compiled from AFM image analysis for over 225 separate nanotubes, with the exact number, *N*, shown for each histogram. The average attachment probabilities, *p*, used to generate the calculated binomial distributions are indicated for each case.

consequently, a larger spacing than expected, that is, 29 and 14 nm, respectively. Additionally, successful attachment of 15 quantum dots to a DNA nanotube functionalized with 29 biotin binding sites was observed by TEM (see Supporting Information S7). The average quantum dot spacing was measured to be 28 ± 7 nm, in agreement with the average spacing measured by AFM.

In Figure 2, only 10 quantum dots were attached to the nanotube with 15 available sites, and only 17 quantum dots were attached to the nanotube with 29 available sites. It is also noted that for the cases of 15 and 29 binding sites, the attached quantum dots alternate from one side of the DNA nanotube to the other with a greater frequency than for the cases of 5 or 9 binding sites. Several factors, hereafter referred to as binding obstructions, that may limit quantum dot attachment include (1) steric hindrance between quantum dots, (2) quantum dots bridging multiple biotin-labeled staple strands, (3) site poisoning of biotin-labeled staple strands by free streptavidin, (4) biotin-labeled staple strands that are missing their biotin modification, and (5) trapping of tethered biotin inside the DNA nanotube. Based on the design of the DNA nanotubes, 15 and 29 binding sites correspond to periodicities of 29 and 14 nm, respectively. AFM measurements of the center-to-center quantum dot separation show a minimum separation distance of 20 nm, which we interpret as the effective diameter of the quantum dots in solution (see Supporting Information S8). Thus, steric hindrance is expected for an array periodicity of 20 nm or less (e.g., 14 nm).

To further assess the degree of successful quantum dot attachment, Figure 3 shows histograms of the number of quantum dots attached to DNA nanotubes labeled with (a) 5, (b) 9, (c) 15, and (d) 29 biotin binding sites. The data for the histograms were compiled from AFM image analysis for over 225 separate nanotubes for each case (see Supporting Information S9). For the cases of 5 and 9 available binding sites, the histograms are peaked at 4 and 7 successful attachments, very near the designed number of sites. However, in the cases of 15 and 29 available sites, the histograms are peaked at 10 and 17 successful attachments, confirming that attachment to each available binding site is much more likely for nanotubes functionalized with 5 or 9 binding sites than for those with 15 or 29. It is also noted that a small number of nanotubes appeared to have more attached quantum dots than available binding sites, which we attribute to coincidental alignment of a nanotube with full attachment and free quantum dots.

Assuming that quantum dot binding events occur with an equal average attachment probability for each site, the attachment histograms would be expected to follow a binomial distribution, $P(m)$, given by

$$P(m) = \frac{n!}{m!(n-m)!} p^m (1-p)^{(n-m)} \qquad (1)$$

where n is the given number of available biotin binding sites per nanotube and m is the number of attached quantum dots per nanotube.[52] The average attachment probability, p, is given by

DOI: 10.1021/nl101079u | *Nano Lett.* **2010,** *10,* 3367–3372

$$p = \frac{\sum \text{attached QD}}{\sum \text{available sites}} \quad (2)$$

where the numerator is the total number of attached quantum dots, and the denominator is the total number of available attachment sites. The average attachment probabilities were calculated using eq 2 from the histogram data to be 0.77, 0.76, 0.65, and 0.64 for 5, 9, 15, and 29 sites, respectively. For the case of 5 binding sites, the attachment probability for pure streptavidin was calculated from histogram data to be 0.79, only slightly higher than for quantum dot attachment (see Supporting Information S10). Similar attachment probabilities for pure streptavidin and quantum dots may indicate biotin-labeled staple strands are missing their biotin modification and/or tethered biotin is trapped inside the DNA nanotube. The solid lines in Figure 3 plot the calculated binomial distribution of eq 1 for each case. Overall, the calculated distributions follow the data well, confirming equal attachment probability per site. However, the histograms in Figure 3c,d display a slight shift toward lower attachment, providing some evidence for steric hindrance or site bridging.

For evidence of steric hindrance or bridging, the nearest-neighbor separation distances, projected along the nanotube axis, were measured for pairs of bound quantum dots (see Supporting Information S11). In the absence of steric hindrance or site bridging, the nearest-neighbor separation histograms would be expected to follow a geometric distribution peaked at the designed nanotube binding site periodicity. The geometric distribution, $P(l)$, of nearest-neighbor separations is given by

$$P(l) = p(1 - p)^{(l-1)} \quad (3)$$

where l is the integer number of periods between nearest-neighbors.[52] Histograms of the nearest-neighbor separations and the geometric distributions calculated using the average attachment probabilities p are shown in Figure 4 for each of the four cases. For each case, measured nearest-neighbor separation distances were normalized to represent the number of designed binding site periods between particles. The data were sorted into bins of width a centered on the n^{th} period, where a is the designed nanotube periodicity and n is an integer. Thus, nearest-neighbor separations of less than $a/2$ were indicated as a zero separation. For 5 and 9 attachment sites, the nearest-neighbor separation histograms are peaked at the designed binding site periodicity. However, for 15 and 29 binding sites, the nearest-neighbor separation histograms are peaked at 2 and 3 periods, respectively. The calculated geometric distributions match the data well for the nanotubes with 5 and 9 attachment sites, but deviate significantly for the nanotubes with 15 and 29 sites. Thus, the data may indicate that steric hindrance or site bridging reduce the number of quantum dots attached to the nanotubes.

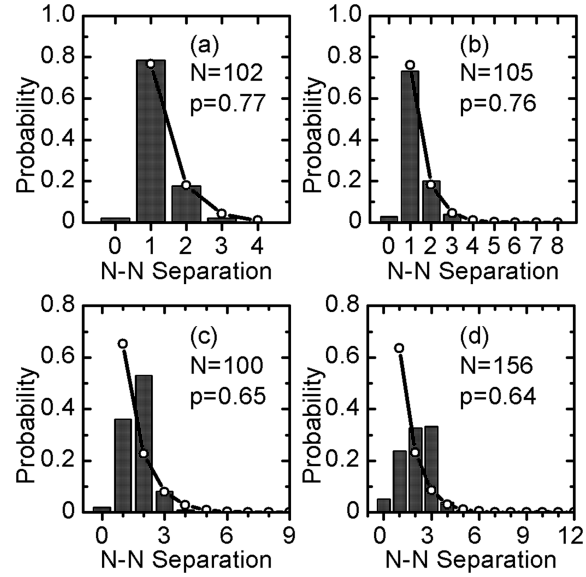

FIGURE 4. Histograms (bars) and calculated geometric distributions (lines) for nearest-neighbor (N-N) separation of bound quantum dot pairs for DNA nanotubes with (a) 5, (b) 9, (c) 15, and (d) 29 biotin binding sites. The numbers of separations, *N*, measured for each case are provided in the figures, along with the average attachment probabilities, *p*. N-N separation of zero indicates two nearest neighbors with a separation less than one-half of a period.

Functionalized DNA origami nanotubes were designed with biotin-labeled staple strands spaced evenly along the axis of the nanotubes. The nanotubes were synthesized and combined with streptavidin-conjugated quantum dots to form nanoparticle arrays with controlled periodicities. AFM images of the synthesized arrays revealed successful attachment of quantum dots at locations along the nanotube axes that corresponded to available biotin binding sites. Statistical analysis of AFM images indicates that binding obstructions establish an upper limit on the yield of nanotubes fully occupied by quantum dots, as indicated by reduced attachment probabilities and deviations from the expected nearest-neighbor distributions for nanotubes with 15 or 29 binding sites. In addition to steric hindrance between quantum dots and quantum dots bridging multiple biotin-labeled staple strands, obstructions may include (1) site poisoning of biotin-labeled staple strands by free streptavidin, (2) biotin-labeled staple strands that are missing their biotin modification, and (3) trapping of tethered biotin inside the DNA nanotube. In addition, a minimum gap distance was measured between two streptavidin-conjugated quantum dots, thereby establishing an important design constraint when fabricating nanoelectronic and nanoplasmonic devices based on DNA origami.

These results provide a powerful and convenient pathway to control nanoparticle patterning, allowing for self-as-

DOI: 10.1021/nl101079u | *Nano Lett.* **2010,** *10,* 3367–3372

sembled fabrication of nanoscale electronic and photonic devices. Because of the symmetry of DNA origami nanotubes and the nonrepeating sequence of the scaffold strand, it is possible to extend the nanotube functionalization technique to form aperiodic arrays, as well as three-dimensional arrays. Considering there are 170 unique staple strands that can be functionalized by various means at either end, or even within the strand itself, the possibilities for variations are vast. Inclusion of nanoparticles of differing size and/or differing material is within reach and extended networks of functionalized DNA origami nanotubes linked together in two or even three dimensions is plausible.

Acknowledgment. The authors are grateful to Dr. Paul W. K. Rothemund for stimulating discussions, Chad Watson for AFM support, Colin Green for acquiring the TEM data included in the Supporting Information S7, and Ross Butler for writing the Perl script included in the Supporting Information S2. This work was supported in part by DARPA Contract No. N66001-01-C-80345, NIH Grant P20 RR016454 from the INBRE Program of the National Center for Research Resources, NSF CCF Grant 0855212, and NSF CAREER Grant ECCS-0846415. The TEM work was performed in the Boise State Center for Materials Characterization and supported by the NSF MRI Grant No. DMR-0521315. The AFM work was supported in part by the NSF MRI Grant No. ECCS-0216312.

Supporting Information Available. Design schematics and strand sequences for the DNA nanotubes, identification of biotinylated sequences, AFM calibration, and details of AFM, TEM, and statistical image analysis. This material is available free of charge via the Internet at http://pubs.acs.org.

REFERENCES AND NOTES

(1) Lin, C.; Liu, Y.; Rinker, S.; Yan, H. *ChemPhysChem* **2006**, *7*, 1641–1647.
(2) Stewart, M. E.; Anderton, C. R.; Thompson, L. B.; Maria, J.; Gray, S. K.; Rogers, J. A.; Nuzzo, R. G. *Chem. Rev.* **2008**, *108*, 494–521.
(3) Zhao, Y.; Thorkelsson, K.; Mastroianni, A. J.; Schilling, T.; Luther, J. M.; Rancatore, B. J.; Matsunaga, K.; Jinnai, H.; Wu, Y.; Poulsen, D.; Fréchet, J. M. J.; Alivisatos, A. P.; Xu, T. *Nat. Mater.* **2009**, *8*, 979–985.
(4) Mirkin, C. A.; Letsinger, R. L.; Mucic, R. C.; Storhoff, J. J. *Nature* **1996**, *382*, 607–609.
(5) Xu, X.; Rosi, N. L.; Wang, Y.; Huo, F.; Mirkin, C. A. *J. Am. Chem. Soc.* **2006**, *128*, 9286–9287.
(6) Nykypanchuk, D.; Maye, M. M.; van der Lelie, D.; Gang, O. *Nature* **2008**, *451*, 549–552.
(7) Park, S. Y.; Lytton-Jean, A. K. R.; Lee, B.; Weigand, S.; Schatz, G. C.; Mirkin, C. A. *Nature* **2008**, *451*, 553–556.
(8) Alivisatos, A. P.; Johnsson, K. P.; Peng, X.; Wilson, T. E.; Loweth, C. J.; Bruchez, M. P., Jr.; Schultz, P. G. *Nature* **1996**, *382*, 609–611.
(9) Loweth, C. J.; Caldwell, W. B.; Peng, X.; Alivisatos, A. P.; Schultz, P. G. *Angew. Chem., Int. Ed.* **1999**, *38*, 1808–1812.
(10) Fu, A.; Micheel, C. M.; Cha, J.; Chang, H.; Yang, H.; Alivisatos, A. P. *J. Am. Chem. Soc.* **2004**, *126*, 10832–10833.
(11) Aldaye, F. A.; Sleiman, H. F. *J. Am. Chem. Soc.* **2007**, *129*, 4130–4131.
(12) Aldaye, F. A.; Sleiman, H. F. *Angew. Chem., Int. Ed.* **2006**, *45*, 2204–2209.
(13) Lee, J. H.; Wernette, D. P.; Yigit, M. V.; Liu, J.; Wang, Z.; Lu, Y. *Angew. Chem., Int. Ed.* **2007**, *46*, 9006–9010.
(14) Niemeyer, C. M.; Bürger, W.; Peplies, J. *Angew. Chem., Int. Ed.* **1998***37*, 2265–2268.
(15) Deng, Z.; Tian, Y.; Lee, S. H.; Ribbe, A. E.; Mao, C. *Angew. Chem., Int. Ed.* **2005**, *44*, 3582–3585.
(16) Beyer, S.; Nickels, P.; Simmel, F. C. *Nano Lett.* **2005**, *5*, 719–722.
(17) Seeman, N. C. *Nature* **2003**, *421*, 427–431.
(18) Seeman, N. C. *Mol. Biotechnol.* **2007**, *37*, 246–257.
(19) Aldaye, F. A.; Palmer, A. L.; Sleiman, H. F. *Science* **2008**, *321*, 1795–1799.
(20) Lin, C.; Liu, Y.; Yan, H. *Biochemistry* **2009**, *48*, 1663–1674.
(21) Chen, J.; Seeman, N. C. *Nature* **1991**, *350*, 631–633.
(22) Winfree, E.; Liu, F.; Wenzler, L. A.; Seeman, N. C. *Nature* **1998**, *394*, 539–544.
(23) Shih, W. M.; Quispe, J. D.; Joyce, G. F. *Nature* **2004**, *427*, 618–621.
(24) Rothemund, P. W. K.; Nkodo, A. E.; Papadakis, N.; Kumar, A.; Fygenson, D. K.; Winfree, E. *J. Am. Chem. Soc.* **2004**, *126*, 16344–16352.
(25) Rothemund, P. W. K. *Nature* **2006**, *440*, 297–302.
(26) Kuzuya, A.; Komiyama, M. *Nanoscale* **2010**, *2*, 310–322.
(27) Shih, W. M.; Lin, C. *Curr. Opin. Struct. Biol.* **2010**, *20*, 276–282.
(28) Le, J. D.; Pinto, Y.; Seeman, N. C.; Musier-Forsyth, K.; Taton, T. A.; Kiehl, R. A. *Nano Lett.* **2004**, *4*, 2343–2347.
(29) Zhang, J.; Liu, Y.; Ke, Y.; Yan, H. *Nano Lett.* **2006**, *6*, 248–251.
(30) Zheng, J.; Constantinou, P. E.; Micheel, C.; Alivisatos, A. P.; Kiehl, R. A.; Seeman, N. C. *Nano Lett.* **2006**, *6*, 1502–1504.
(31) Sharma, J.; Chhabra, R.; Liu, Y.; Ke, Y.; Yan, H. *Angew. Chem., Int. Ed.* **2006**, *45*, 730–735.
(32) Sharma, J.; Chhabra, R.; Andersen, C. S.; Gothelf, K. V.; Yan, H.; Liu, Y. *J. Am. Chem. Soc.* **2008**, *130*, 7820–7821.
(33) Sharma, J.; Ke, Y.; Lin, C.; Chhabra, R.; Wang, Q.; Nangreave, J.; Liu, Y.; Yan, H. *Angew. Chem., Int. Ed.* **2008**, *47*, 5157–5159.
(34) Hung, A. M.; Micheel, C. M.; Bozano, L. D.; Osterbur, L. W.; Wallraff, G. M.; Cha, J. N. *Nat. Nanotechnol.* **2010**, *5*, 121–126.
(35) Pal, S.; Deng, Z.; Ding, B.; Yan, H.; Liu, Y. *Angew. Chem., Int. Ed.* **2010**, *49*, 2700–2704.
(36) Ding, B.; Deng, Z.; Yan, H.; Cabrini, S.; Zuckermann, R. N.; Bokor, J. *J. Am. Chem. Soc.* **2010**, *132*, 3248–3249.
(37) Sharma, J.; Chhabra, R.; Cheng, A.; Brownell, J.; Liu, Y.; Yan, H. *Science* **2009**, *323*, 112–116.
(38) Mitchell, G. P.; Mirkin, C. A.; Letsinger, R. L. *J. Am. Chem. Soc.* **1999**, *121*, 8122–8123.
(39) Mathieu, F.; Liao, S.; Kopatsch, J.; Wang, T.; Mao, C.; Seeman, N. C. *Nano Lett.* **2005**, *5*, 661–665.
(40) Douglas, S. M.; Chou, J. J.; Shih, W. M. *Proc. Natl. Acad. Sci.* **2007**, *104*, 6644–6648.
(41) Morris, V. J.; Kirby, A. R.; Gunning, A. P. *Atomic Force Microscopy for Biologists*; Imperial College Press: London, 1999.
(42) Hertel, T.; Walkup, R. E.; Avouris, P. *Phys. Rev. B* **1998**, *58*, 13870–13873.
(43) Weisenhorn, A. L.; Khorsandi, M.; Kasas, S.; Gotzos, V.; Butt, H. J. *Nanotechnology* **1993**, *4*, 106–113.
(44) Weisenhorn, A. L.; Schmitt, F.-J.; Knoll, W.; Hansma, P. K. *Ultramicroscopy* **1992**, *42−44*, 1125–1132.
(45) Perrson, B. N. J. *Chem. Phys. Lett.* **1987**, *141*, 366–368.
(46) Weisenhorn, A. L.; Drake, B.; Prater, C. B.; Gould, S. A. C.; Hansma, P. K.; Ohnesorge, F.; Egger, M.; Heyn, S. P.; Gaub, H. E. *Biophys. J.* **1990**, *58*, 1251–1258.
(47) Gould, S. A. C.; Drake, B.; Prater, C. B.; Weisenhorn, A. L.; Manne, S.; Hansma, H. G.; Hansma, P. K.; Massie, J.; Longmire, M.; Elings, V.; Dixon Northern, B.; Mukergee, B.; Peterson, C. M.; Stoeckenius, W.; Albrecht, T. R.; Quate, C. F. *J. Vac. Sci. Technol., A* **1990**, *8*, 369–373.
(48) Wilcheck, M.; Bayer, E. A. *Avidin/biotin technology, Methods in Enzymology*; Academic Press: San Diego, 1990; Vol. 184.
(49) Hendrickson, W. A.; Pähler, A.; Smith, J. L.; Satow, Y.; Merritt, E. A.; Phizackerley, R. P. *Proc. Natl. Acad. Sci. U.S.A.* **1989**, *86*, 2190–2194.
(50) Weber, P. C.; Ohlendorf, D. H.; Wendoloski, J. J.; Salemme, F. R. *Science* **1989**, *243*, 85–88.
(51) Busse, S.; Scheumann, V.; Menges, B.; Mittler, S. *Biosens. Bioelectron.* **2002**, *17*, 704–710.
(52) Mendenhall, W.; Scheaffer, R. L. *Mathematical Statistics with Applications*; Duxbury Press: North Scituate, MA, 1972.

DOI: 10.1021/nl101079u | *Nano Lett.* **2010,** *10,* 3367–3372

(SUPPORTING INFORMATION)

Programmable Periodicity of Quantum Dot Arrays with DNA Origami Nanotubes

Hieu Bui, [†] Craig Onodera, [‡] Carson Kidwell, [‡] YerPeng Tan, [‡] Elton Graugnard, [‡] Wan Kuang, [†] Jeunghoon Lee, [§] William B. Knowlton, [†,‡] Bernard Yurke, [†,‡] and William L. Hughes *[,‡]

[†] Department of Electrical and Computer Engineering, [‡] Department of Materials Science and Engineering, and [§] Department of Chemistry and Biochemistry, Boise State University, Boise ID 83725

* To whom correspondence should be addressed: WillHughes@BoiseState.edu

SUPPORTING INFORMATION S1: *DNA Nanotube Design*

The DNA nanotubes reported here consist of six parallel double helices that are formed into a tube structure by combining the single-stranded M13mp18 DNA molecule with 170 staple strands using the DNA origami method of Rothemund.[25] As shown in Fig. S1(a), the scaffold is arranged into six numbered helices with the ends of the M13mp18 located in the middle of helix 1. From the 5' end, the scaffold proceeds to the left with crossovers at the ends of the nanotube and two staggered crossovers near the middle. The nucleotide numbers for the crossovers are indicated in the figure. Staple strands are grouped into 86 columns and numbered from the left end, as shown in Fig. S1(b). Staples are labeled according to the helix and column location of their 5' end. The first column of staples starts 14 nucleotides from the left end scaffold crossovers. Columns 11-13 show the 3 column repeating motif in which each staple consists of three 14 nucleotide domains complementary to a section of the M13mp18 scaffold and spans 3 helices. Although not used in the current study, three random 20 nucleotide sticky-ends, labeled A, B, and C, are added to staples in columns 4, 7, and 10 of helix 3. For each sticky-end, the helix 3 domain complementary to M13mp18 is lengthened by 7 nucleotides and the adjacent staple domain is correspondingly shortened, as illustrated in the figure.

The staple strand layout in the middle of the nanotube is shown in Fig. S1(c). The 5' and 3' ends of the M13mp18 scaffold are located in helix 1 and staple column 43. Mid-nanotube scaffold crossovers are located in staple columns 39 and 41. The same A, B, and C sticky-ends are added to staples in columns 41, 45, and 48 of helix 3. Figure S1(d) illustrates the staple layout for the right end of the nanotube. A, B, and C sticky-ends are added to staples of columns 77, 80, and 83 of helix 3. Four nucleotides remain unhybridized at the end of each helix. A schematic of the formed DNA nanotube with A, B, and C sticky-ends is shown in Fig. S1(e).

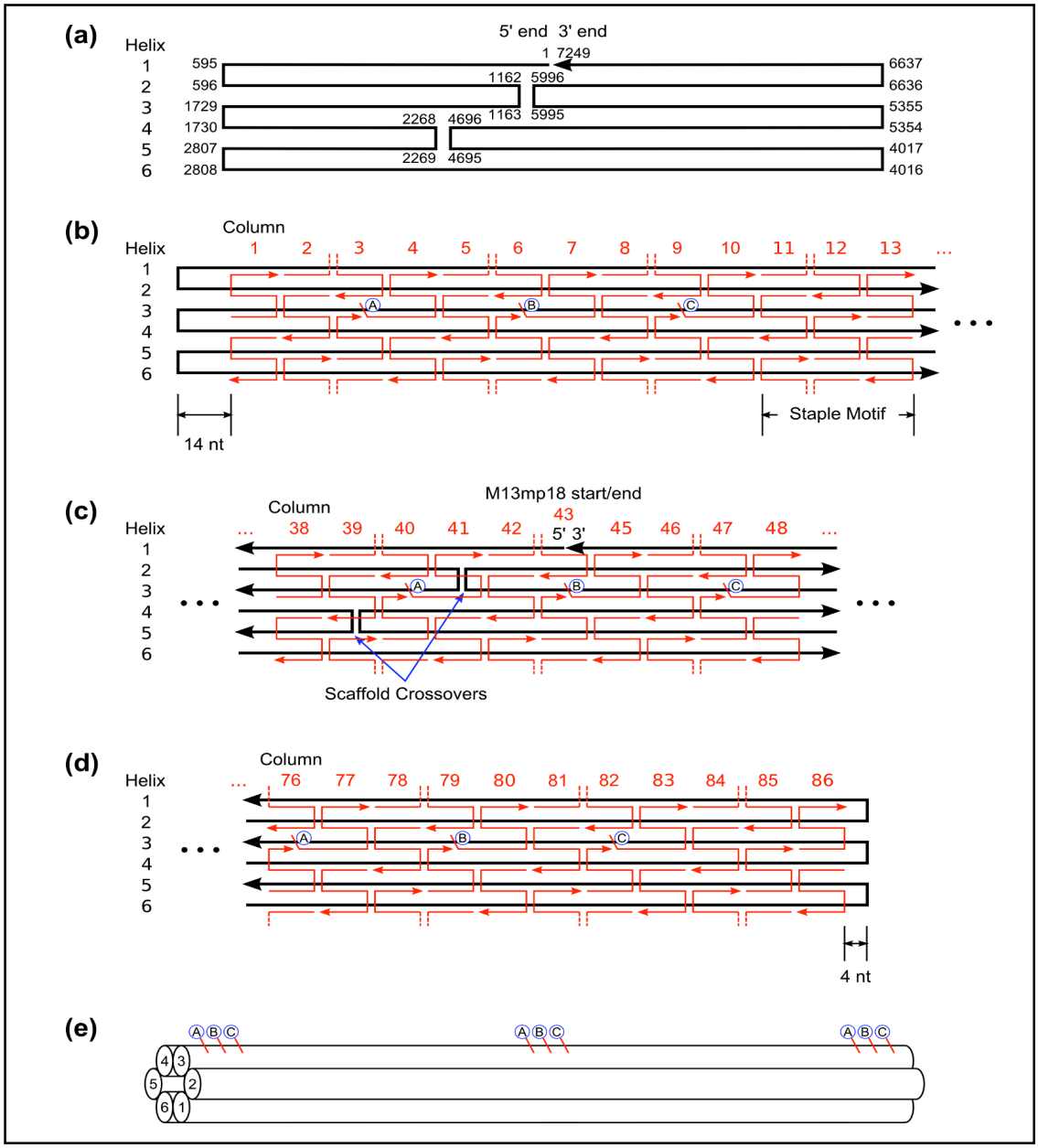

FIGURE S1. Two-dimensional layout of the scaffold and staple strands of the DNA nanotube and 3D schematic. (a) Layout of the scaffold showing nucleotide numbers at the crossovers. (b) Staple layout for the left end of the tube. The staple motif is shown in columns 11-13. In helix 3, staples in columns 4, 7, and 10 are extended with sticky-ends labeled A, B, and C. (c) Staple layout in the middle of the tube. The M13mp18 scaffold begins and ends in helix 1, column 43. Scaffold crossovers are located at the ends and in columns 39 and 41. A,B, and C sticky-ends are added to staples 41, 45, and 48 of helix 3. (d) Staple layout for the right end of the tube. Sticky-ends are added to staples in helix 3 in columns 77, 80, and 83. Four nucleotides remain at the end of each helix. (e) Schematic of the formed tube illustrating the A, B, and C sticky-ends along helix 3 of the formed nanotube.

SUPPORTING INFORMATION S2: *DNA Nanotube Staple Strands*

To facilitate generation of the staple strands required to form a 6-helix DNA nanotube, a Perl script was written to layout the scaffold sequence into the geometric raster pattern according to a given set of turning points. The script accepts the M13mp18 sequence as an input, divides the sequence into regions demarcated by turning points, and then outputs the scaffold and its complement according to the designed pattern. The complementary sequence is then easily divided into staple strands according to the desired motif.

Perl Script:

```
################################################################
#                                                              #
#               DNA Origami Design Helper Program              #
#                                                              #
#                    Boise State University                    #
#                                                              #
################################################################

use strict;
use warnings;
use English;
use Carp;

exit(main());                          # a nice technique for avoiding global variables in Perl

sub main {

    my $DNA_SEQUENCE_FILENAME = 'M13mp18BP.txt';

    # Read the dna sequence data from the file named in $DNA_SEQUENCE_FILENAME.
    my $DNA_SEQUENCE_FILE;
    if (!open($DNA_SEQUENCE_FILE, "< $DNA_SEQUENCE_FILENAME")) {
        print "Unable to open data file $DNA_SEQUENCE_FILENAME\n";
        return 1;                                       # failure
    }
    my @seqLines = <$DNA_SEQUENCE_FILE>;                # read the dna sequence data lines into
                                                        # the seqLines array
    close $DNA_SEQUENCE_FILE;
    {
        local $INPUT_RECORD_SEPARATOR = "\r\n";         # Temporarily change the record separator so that
        chomp (@seqLines);                              # we can get rid of the line ending characters that
                                                        # are found in text files created on Windows.
    }
    my $n = scalar(@seqLines);
    print "Read $n lines from file $DNA_SEQUENCE_FILENAME.\n";

    # Convert the file data into an array of bases.
    shift @seqLines;                                    # discard the header line
    map { $_ =~ s/[^GATC]+//g } @seqLines;              # discard everything that isn't a G, A, T, or C
    my $dnaSequence = join '', @seqLines;               # concatenate the lines into one big string
    print 'dnaSequence has ' . length($dnaSequence) . " bases.\n";

    # The scaffold structure is described as a set of lines and turnaround points.
    # Data structure:  arefSubsequenceLines -> arefSubsequenceRanges -> [startPos, endPos]
    my $arefSubsequenceLines = [
        [ [ 595,    1], [7249, 6637] ],
        [ [ 596, 1162], [5996, 6636] ],
        [ [1729, 1163], [5995, 5355] ],
        [ [1730, 2268], [4686, 5354] ],
        [ [2807, 2269], [4685, 4017] ],
        [ [2808, 4016],              ],
    ];
```

```
    # Use the position data to divide the DNA sequence into the
    # base pair sequences that make up each line of the structure.
    my @designLines;
    foreach my $arefSubsequenceRanges (@$arefSubsequenceLines) {
        my $designLine = "";
        foreach my $arefSubsequenceRange (@$arefSubsequenceRanges) {
            my ($p1, $p2) = @$arefSubsequenceRange;i8i8sx
            print "p1=$p1, p2=$p2; ";
            if ($p1 <= $p2) {           # don't need to reverse the subsequence?
                                        # (i.e., should appear left to right?)
                $designLine .= "*" if length($designLine) && $p1 != 1;  # separate subsequences
                                                                        # with an asterisk
                $designLine .= substr $dnaSequence, $p1-1, $p2-$p1+1;
            }
            else {                      # must reverse the subsequence because it must
                                        # appear right to left
                $designLine .= "*" if length($designLine) && $p2 != 1;  # separate subsequences
                                                                        # with an asterisk
                $designLine .= reverse substr $dnaSequence, $p2-1, $p1-$p2+1;
            }
            print "length(designLine)=" . length($designLine) . "\n";
        }
        push @designLines, $designLine;
        print "\n";
    }

    my $DESIGN_OUTPUT_FILE;
    if (!open($DESIGN_OUTPUT_FILE, "> tubedesign.txt")) {
        print "Unable to open output file tubedesign.txt\n";
        return 1;                           # failure
    }

    my $COMP_DESIGN_OUTPUT_FILE;
    if (!open($COMP_DESIGN_OUTPUT_FILE, "> comptubedesign.txt")) {
        print "Unable to open output file comptubedesign.txt\n";
        return 1;                           # failure
    }

    # Format the output lines as needed for the next design step.
    foreach my $designLine (@designLines) {

        my $outputLine = $designLine;

        $outputLine =~ s/([GATC]{7})\*([GATC]{7})/ $1*$2 /;     # create a 7+7 subsequence at
                                                                # the turnaround points
        $outputLine =~ s/([GATC]{14})/$1 /g;                    # break everything else into
                                                                # 14-base subsequences
        $outputLine =~ s/ {3,}/  /g;                            # make sure there are no more
                                                                # than 2 consecutive spaces
        $outputLine =~ s/  $//;                                 # get rid of the dangling spaces
                                                                # at the end of the line

        # Create the complements.
        my $complementLine = $outputLine;
        $complementLine =~ s/G/c/g;
        $complementLine =~ s/C/g/g;
        $complementLine =~ s/A/t/g;
        $complementLine =~ s/T/a/g;
        $complementLine = uc $complementLine;

        print $DESIGN_OUTPUT_FILE "$outputLine\n$complementLine\n\n";
        print $COMP_DESIGN_OUTPUT_FILE "$complementLine\n\n";
    }

    close $DESIGN_OUTPUT_FILE;
    close $COMP_DESIGN_OUTPUT_FILE;

    return 0;                               # success
}
```

Table S1 provides the name and sequence for the 170 unique staple strands used for the 6-helix DNA nanotube reported here. The names are derived from the helix and column location of the 5' end of the staple strand, as described in S1. There are 152 strands with 42 nucleotides consisting of 3 domains each 14 nucleotides in length. Nine strands are 69 nucleotides in length, consisting of a helix-3 domain lengthened by 7 nucleotides plus a random 20 nucleotide sticky-end sequence. Nine strands adjacent to the lengthened staples are shortened by 7 nucleotides leaving 35 nucleotides.

TABLE S1: Name and sequence for the 170 staple strands used for the 6-helix DNA nanotube.

Helix	Column	Sequence
1	2	GCCAGAGGGGGTAAAGACTCCTTATTACAACGCAAAGACACC
1	5	CAATACTGCGGAATAACGCAATAATAACATAGAAAATTCATA
1	8	AAATGCTTTAAACATAAGCAGATAGCCGCGACATTCAACCGA
1	11	AAAAATCAGGTCTTAAATAGCAATAGCTAAATTATTCATTAA
1	14	GCGGATTGCATCAACAAGAATTGAGTTAGCCATTTGGGAATT
1	17	CAAATATCGCGTTTAGTCAGAGGGTAATTTACCATTAGCAAG
1	20	GGAAGCAAACTCCAGAAGCGCATTAGACATAGCAGCACCGTA
1	23	TTGCTCCTTTTGATTGAAAATAGCAGCCTTAGCGTCAGACTG
1	26	GCTTAATTGCTGAACCCAATCCAAATAAATAGCCCCCTTATT
1	29	ATATGCAACTAAAGGCCTAATTTGCCAGTCACCGGAACCAGA
1	32	AACAGTTGATTCCCTTTATCCTGAATCTCCGCCACCCTCAGA
1	35	ACCATTAGATACATCCTTAAATCAAGATGAGCCGCCACCAGA
1	38	TATATTTTCATTTGAGGCGTTTTAGCGAACAGGAGTTAGACT
1	41	TCTACTAATAGTAGCAAATCAGATATAGATCCTTTGCCCGAA
1	44	GCAAGGCAAAGAATTTTATTTTCATCGTATTATCATTTTGCG
1	47	GCATAAAGCTAAATATTAAACCAAGTACATTATCATCATATT
1	50	TAATACTTTTGCGGATCAATAATCGGCTAATATAATCCTGAT
1	53	AAAATTTTTAGAACAAAAATAATATCCCAGGGTTAGAACCTA
1	56	GTAATGTGTAGGTAAGAACGCGCCTGTTAGAAATAAAGAAAT
1	59	GACAGTCAAATCACTCTGTCCAGACGACTGAATATACAGTAA
1	62	TGATAAATTAATGCAGTAATAAGAGAATAACGGATTCGCCTG
1	65	TACAAAGGCTATCAAACAACGCCAACATGCGCAGAGGCGAAT
1	68	AAGAGAATCGATGACCAACGCTCAACAGAGATGATGAAACAA
1	71	CATATGTACCCCGGTTTAGTATCATATGTAACAATTTCATTT
1	74	GAAGATTGTATAAGATAAGAATAAACACATAAATCAATATAT
1	77	TTTGTTAAAATTCGTAATGGTTTGAAATCGTCGCTATTAATT
1	80	TTTTAACCAATAGGTTTCAAATATATTTAGCGATAGCTTAGA
1	83	CCTTCCTGTAGCCATGATGCAAATCCAAATTTATCAAAATCA
2	2	TATCATAACCCTCGCGTCTTTCCAGACGGTACAAACTACAAC
2	5	CATAACGCCAAAAGTTGCTAAACAACTTCCAATAGGAACCCA
2	8	TCAGTTGAGATTTAAAGGAACAACTAAACCACCCTCAGAGCC
2	11	AACGAACTAACGGATGAAAATCTCCAAAGGTTTAGTACCGCC
2	14	TATACCAGTCAGGAGTATCGGTTTATCAATATAAGTATAGCC
2	17	ATCATTGTGAATTAAGCTTGATACCGATTTTTGCTCAGTACC
2	20	CGAGTAGTAAATTGGCCCACGCATAACCAGAGGCTGAGACTC
2	23	TCATTCAGTGAATAGAGTTAAAGGCCGCTGCCTATTTCGGAA
2	26	AGAACCGGATATTCAAAGACAGCATCGGGTGCCTTGAGTAAC
2	29	GGCGCATAGGCTGGTTGAGGACTAAAGAGATGATACAGGAGT
2	32	TGACCAACTTTGAAGGGTAAAATACGTATCTCTGAATTTACC
2	35	GCCGGAACGAGGCGCGAAAGAGGCAAAACAAACAAATAAATC
2	38	GATAAATTGTGTCGCCCAGCGATTATACAGAAGTAGTTGAGG
2	41	TTTGCGTATTGGGCTCTTTTCACCAGTGTAATAGATTAGAGC
2	44	CCAGCTGCATTAATCGCCTGGCCCTGAGTTGAGGAAGGTTAT
2	47	GTTGCGCTCACTGCTTGCCCCAGCAGGCAATCAATATCTGGT

2	50	AGCCTGGGGTGCCTATCGGCAAAATCCCATCTAAAGCATCAC
2	53	CACAATTCCACACAGGGTTGAGTGTTGTGCCTGCAACAGTGC
2	56	ATCATGGTCATAGCAAGAACGTGGACTCAGCAGAAGATAAAA
2	59	GTCGACTCTAGAGGCAGGGCGATGGCCCTAGCCCTAAAACAT
2	62	CGTTGTAAAACGACTTTTTGGGGTCGAGCAATATTTTTGAAT
2	65	AGGCGATTAAGTTGAAAGGGAGCCCCCGAGAACCCTTCTGAC
2	68	TCTTCGCTATTACGAACGTGGCGAGAAACACACGACCAGTAA
2	71	TTCAGGCTGCGCAAGCTAGGGCGCTGGCAATCGTCTGAAATG
2	74	ACCGCTTCTGGTGCACCACACCCGCCGCAACAGGAAAAACGC
2	77	GTATCGGCCTCAGGTATGGTTGCTTTGACTTGCTGGTAATAT
2	80	GCATCGTAACCGTGAGAATCAGAGCGGGAATAACATCACTTG
2	83	GGATTGACCGTAATTTTAGACAGGAACGATCACGCAAATTAA
3	1	ATCTAAAGTTTTGTTTTACCAGACGACGGCAAAAGAAGTTTT
3	4	GAACGCACTTGGTCTACTGAATGAATTTTCTGTATGGGATTGAATTACGAGGCATGACTGGATAGCGTC
3	7	GTGACATACCTTCGGAGCATTTTCAGCGGAGTGAGAATAGAGGAATACCACATTCATTGAATCCCCCTC
3	10	CGCTTCACGAGGTTACAATGCGAATAATAATTTTTTCACGTACAACATTATTACAAATGACCATAAATC
3	13	AGGAGCCTTTAATTCGTTGGGAAGAAAATAGTCAGAAGCAAA
3	16	TGAATTTCTTAAACCCTTATGCGATTTTAGCCCGAAAGACTT
3	19	TGACAACAACCATCGGCTTGAGATGGTTAAGCGAACCAGACC
3	22	CTGAGGCTTGCAGGAGGCTTGCCCTGACGAGAGTACCTTTAA
3	25	CACCCTCAGCAGCGATTACCCAAATCAAGCGGATGGCTTAGA
3	28	CGGCTACAGAGGCTCTGACCTTCATCAATCAACATGTTTTAA
3	31	AGTTTCCATTAAACAGAGGACAGATGAAGTTTCATTCCATAT
3	34	GCACCAACCTAAAACAGACGGTCAATCAGTAGATTTAGTTTG
3	37	ACTCATCTTTGACCAAATCCGCGACCTGATAACCTGTTTAGC
3	40	GAACGCACTTGGTCTACTGAGAAACAAAGTACAATGGTTTTGCCAGGGCGGAGATAAGGTGGCATCAAT
3	43	GTGACATACCTTCGGAGCATCAACAGCTGATTGCCCTTCACGAATCGGCCAACGCAATAAATCATACAG
3	46	CGCTTCACGAGGTTACAATGCAGCAAGCGGTCCACGCTGGTCCGCTTTCCAGTCGAATAAAGCCTCAGA
3	49	ATGGTGGTTCCGAAAATGAGTGAGCTAAACATTATGACCCTG
3	52	AATAGCCCGAGATAACATACGAGCCGGATCAACGCAAGGATA
3	55	AGAGTCCACTATTATGTTTCCTGTGTGAAATGCAATGCCTGA
3	58	GAAAAACCGTCTATATCCCCGGGTACCGTGAGAAAGGCCGGA
3	61	CACCCAAATCAAGTGGCCAGTGCCAAGCTCAACCGTTCTAGC
3	64	TAAATCGGAACCCTGGTAACGCCAGGGTATTTTTGAGAGATC
3	67	GGGGAAAGCCGGCGCCAGCTGGCGAAAGAGTCTGGAGCAAAC
3	70	CGAAAGGAGCGGGCCTGTTGGGAAGGGCACTAGCATGTCAAT
3	73	CGCTGCGCGTAACCCGGAAACCAGGCAAAGCCCCAAAAACAG
3	76	GAACGCACTTGGTCTACTGAGCGCCGCTACAGGGCGCGTACAAGATCGCACTCCAGTAAACGTTAATAT
3	79	GTGACATACCTTCGGAGCATGTATAACGTGCTTTCCTCGTTCATCTGCCAGTTTGTAAATCAGCTCATT
3	82	CGCTTCACGAGGTTACAATGCAGGAGGCCGATTAAAGGGATGGGATAGGTCACGTTAATTCGCGTCTGG
3	85	TGAGAAGTGTTTTTCGTCGGATTCTCCGTAAATGTGAGCGAG
4	1	GCCTGTAGCATTCCCAACATATAAAAGAGCAGTATGTTAGCA
4	4	TGTACCGTAACACTTTTTGTCACAATCAGGAATACCCAAAAG
4	7	ACCACCCTCATTTTCAAAGACAAAAGGGAACAAAGTTACCAG
4	10	ACCCTCAGAACCGCGTAAATATTGACGGATCTTACCGAAGCC
4	13	CGGAATAGGTGTATCGTCACCGACTTGAAGCCCAATAATAAG
4	16	AGGCGGATAAGTGCCACCAGTAGCACCATGAGCGCTAATATC
4	19	CTCAAGAGAAGGATCAATGAAACCATCGGGGAGAATTAACTG
4	22	CCTATTATTCTGAAAATCAAGTTTGCCTTTTACAGAGAGAAT
4	25	AGTGCCCGTATAAACGGCATTTTCGGTCGAAACGATTTTTTG
4	28	GTACTGGTAATAAGTTTCATAATCAAAATTACAAAATAAACA
4	31	GTTCCAGTAAGCGTCGCCTCCCTCAGAGTACCAACGCTAACG
4	34	CTCATTAAAGCCAGAGCCACCACCCTCATAGTTGCTATTTTG
4	37	CAGGTCAGACGATTCGCCGCCAGCATTGACCTCCCGACTTGC
4	40	CGTCAATAGATAATACAACTCGTATTAAAAGGCTTATCCGGT
4	43	CTAAAATATCTTTAAAAGTTTGAGTAACAGGAATCATTACCG
4	46	CAGTTGGCAAATCACCAGAAGGAGCGGACGCACTCATCGAGA
4	49	CTTGCTGAACCTCAGATGGCAATTCATCGTCTTTCCTTATCA
4	52	CACGCTGAGAGCCATTCTGAATAATGGAATCCTAATTTACGA
4	55	CAGAGGTGAGGCGGTTTGCACGTAAAACTATCAACAATAGAT
4	58	CGCCATTAAAAATAGGTTTAACGTCAGAGACAATAAACAACA
4	61	GGCTATTAGTCTTTTCGGGAGAAACAATATAAAGTACCGACA
4	64	CTGAAAGCGTAAGACAAGTTACAAAATCGTAATTTAGGCAGA
4	67	TAAAAGGGACATTCACCTGAGCAAAAGATAGGGCTTAATTGA

4	70	GATTATTTACATTGAAATTAATTACATTCGTTATACAAATTC
4	73	TCATGGAAATACCTAATGGAAACAGTACCGGAATCATAATTA
4	76	CCAGAACAATATTATTGCTTCTGTAAATACCGACCGTGTGAT
4	79	CCTGAGTAGAAGAAATCCTTGAAAACATTAGTTAATTTCATC
4	82	CCGTTGTAGCAATAAGAGTCAATAGTGATCGCAAGACAAAGA
4	85	TGAGGCCACCGAGTTACCTTTTTAACCTGTTGGGTTATATAA
5	3	ACGGAATAAGTTTAGAGTTTCGTCACCATTAGTAA
5	6	TGGTTTACCAGCGCCAGGGATAGCAAGCTCAACAG
5	9	TTGAGGGAGGGAAGCACCCTCAGAACCGGGAATTG
5	12	AGGTGAATTATCACCACCGTACTCAGGAAAAAAGGCTCCAAA
5	15	AGAGCCAGCAAAATCGTCGAGAGGGTTGGCTTGCTTTCGAGG
5	18	GCCGGAAACGTCACTAGGATTAGCGGGGAGTTGCGCCGACAA
5	21	ATCAGTAGCGACAGACATGAAAGTATTAGATATATTCGGTCG
5	24	TAGCGCGTTTTCATCAGTTAATGCCCCCTTTTGCGGGATCGT
5	27	AGCGTTTGCCATCTTTTTAACGGGGTCAAACGAGGGTAGCAA
5	30	GCCACCACCGGAACCATACATGGCTTTTCTTTTTCATGAGGA
5	33	ACCGCCACCCTCAGAATGGAAAGCGCAGATGCCACTACGAAG
5	36	ACCACCACCAGAGCGGCCTTGATATTCAGAATACACTAAAAC
5	39	TTACAAACAATTCGACATTTGAGGATTTCAAGCGC
5	42	CGTTATTAATTTTAGGAGCACTAACAACAGACGGG
5	45	GAACAAAGAAACCAACAGTTGAAAGGAAAGAGTTG
5	48	CCTGATTATCAGATAATATCAAACCCTCGAAAATCCTGTTTG
5	51	TGTTTGGATTATACGCAGCAAATGAAAATTATAAATCAAAAG
5	54	CCATATCAAAATTATCAGTATTAACACCTCCAGTTTGGAACA
5	57	TGCGTAGATTTTCACCGAACGAACCACCCAACGTCAAAGGGC
5	60	CAGTACCTTTTACAAATGCGCGAACTGAACTACGTGAACCAT
5	63	ATTGCTTTGAATACATACGTGGCACAGAGTGCCGTAAAGCAC
5	66	TATTCATTTCAATTTGGCCAACAGAGATATTTAGAGCTTGAC
5	69	ACATCAAGAAAACAGCAGATTCACCAGTGGAAGGGAAGAAAG
5	72	GAATTACCTTTTTTACATTTTGACGCTCAAGTGTAGCGGTCA
5	75	GTGAGTGAATAACCCCGCCAGCCATTGCGCTTAAT
5	78	AATTTTCCCTTAGACTCAAACTATCGGCCGAGCAC
5	81	TTAAGACGCTGAGACTTCTTTGATTAGTAGCTAAA
5	84	TAGGTCTGAGAGACAAAAGAGTCTGTCCGTACGCCAGAATCC
6	3	AACTGGCATGATTATAGTAAAATGTTTAAGTAAGAGCAACAC
6	6	AAGGAAACCGAGGACGTCATAAATATTCAACTAATGCAGATA
6	9	CTTTTTAAGAAAAGGTTCAGAAAACGAGGGTAGAAAGATTCA
6	12	AGCAAGAAACAATGTACCCTGACTATTAATCTACGTTAATAA
6	15	AGAGAGATAACCCAAAAGATTAAGAGGAAAGAACTGGCTCAT
6	18	AACACCCTGAACAATAATTCGAGCTTCATAATTTCAACTTTA
6	21	AACATAAAAACAGGACAGGTCAGGATTAGAGAAACACCAGAA
6	24	TTTAACGTCAAAAAAAGAGGTCATTTTTCGTAACAAAGCTGC
6	27	GCCATATTATTTATTATAATGCTGTAGCGAGTAATCTTGACA
6	30	AGCGTCTTTCCAGATACGGTGTCTGGAACGGTGTACAGACCA
6	33	CACCCAGCTACAATAATTCTGCGAACGATAAGGGAACCGAAC
6	36	GGGAGGTTTTGAAGTTCGCAAATGGTCACTCCATGTTACTTA
6	39	ATTCTAAGAACGCGGGGCGCGAGCTGAATTGTATCATCGCCT
6	42	CGCCCAATAGCAAGTAGCATTAACATCCGCGGGGAGAGGCGG
6	45	ACAAGCAAGCCGTTTAGCAAAATTAAGCGGAAACCTGTCGTG
6	48	TTCCAAGAACGGGTCGGTTGTACCAAAACTCACATTAATTGC
6	51	GCATGTAGAAACCAGAGAAGCCTTTATTAGCATAAAGTGTAA
6	54	AAGTCCTGAACAAGCCTCATATATTTTAAATTGTTATCCGCT
6	57	TGTTCAGCTAATGCAAGATTCAAAAGGGAGCTCGAATTCGTA
6	60	AAAGGTAAAGTAATCATCAATATGATATTTGCATGCCTGCAG
6	63	GGCATTTTCGAGCCCGGAGAGGGTAGCTTTTCCCAGTCACGA
6	66	GAATCGCCATATTTGGTCATTGCCTGAGGGGGATGTGCTGCA
6	69	TTACCAGTATAAAGACGGTAATCGTAAAGATCGGTGCGGGCC
6	72	CTAGAAAAAGCCTGTTGATAATCAGAAAAGCGCCATTCGCCA
6	75	AAATAAGGCGTTAACAAATATTTAAATTGCCAGCTTTCCGGC
6	78	TTCTGACCTAAATTCATTAAATTTTTGTAGGGGACGACGACA
6	81	ACGCGAGAAAACTTAACGCCATCAAAAATGGTGTAGATGGGC
6	84	CTATATGTAAATGCGCTTTCATCAACATTGGGAACAAACGGC

SUPPORTING INFORMATION S3: *Modified Staple Strands*

To form functionalized DNA nanotubes with 29 attachment sites for streptavidin-conjugated nanoparticles, all 29 staple strands of helix 4 (H4-C1 to H4-C85) were modified by adding a 5 thymine tether to the 3' end followed by a biotin molecule. During synthesis of the nanotubes, these strands were substituted for the corresponding unmodified staple strands. Note that the strands are labeled in helix 4 by the location of their 5' end, but the biotin modified 3' ends are located in helix 6. To synthesize nanotubes with 15, 9 and 5 available binding sites, the subsets of the helix 4 staple strands were substituted. The column numbers of the substituted staple strands are listed below.

For 15 binding sites, every other staple of helix 4 was substituted:
1, 7, 13, 19, 25, 31, 37, 43, 49, 55, 61, 67, 73, 79, 85.

For 9 binding sites, every third staple of helix 4 was substituted, starting with column 7:
7, 16, 25, 34, 43, 52, 61, 70, 79.

For 5 binding sites, every fifth staple of helix 4 was substituted, starting with column 5:
13, 28, 43, 58, 73.

SUPPORTING INFORMATION S4: *AFM Calibration*

To validate the linearity, stability, and accuracy of the piezoelectric scanners, the AFM was calibrated using: 1) a surface topography reference (STR3-1800P, VLSI Standards), and 2) the atomic step height of freshly cleaved, ZYH grade, highly ordered pyrolytic graphite (HOPG, Veeco Metrology). The STR was lithographically fabricated onto a silicon dioxide on silicon die (Model # STR3-1800P) and contained an array of alternating silicon dioxide bars. With a pitch distance of 3 μm in both the X and Y directions, the bars formed 180 nm deep rectangular pits. Following Veeco Metrology guidelines, the AFM Z-axis piezoelectric stack was calibrated for neutral (0 V ± 5 V), extended (50 V ± 5 V), and retracted (-50 V ± 5 V) conditions. As shown in Table S2, a mean step height of 180.4 ± 0.4 nm was measured at 0 V ± 5 V and is well within the 1-2% accuracy specified by the manufacturer. To verify the calibration of the AFM at small length scales, the mean atomic step height of freshly cleaved, ZYH grade, HOPG was measured to be 0.35 nm with a standard deviation of 0.01 nm. Both the tabulated data and an example height image of the graphite step height are shown in Table S3 and Figure S2, respectively. When compared to the accepted 0.34 nm step height of HOPG, the AFM was properly calibrated.[*]

TABLE S2: Calibration of the AFM using a Surface Topography Reference.

Step Height of Surface Topography Reference	**Expected Value (nm)**	**Measured Value (nm)**	**Relative Error (%)**
Neutral Position (0V ± 5V)	180	180.4	0.2
Extended Offset (50V ± 5V)	180	181.6	0.9
Retracted Offset (-50V ± 5V)	180	181.3	0.7

[*] L. Pauling, *The Nature of the Chemical Bond*, p. 235, 3rd. Edition 1960.

TABLE S3: Calibration of the AFM using freshly cleaved, highly ordered pyrolytic graphite (HOPG).

Number of HOPG Steps	Expected Value (nm)	Measured Value (nm)	Relative Error (%)
1	0.34	0.36	4.7
2	0.34	0.34	0.3
3	0.34	0.33	2.4
4	0.34	0.34	0.6
5	0.34	0.35	3.5
6	0.34	0.35	2.1
7	0.34	0.38	10.9
8	0.34	0.35	1.8
9	0.34	0.34	0.6
10	0.34	0.33	2.1
11	0.34	0.35	2.4
12	0.34	0.34	0.0
13	0.34	0.33	1.8
14	0.34	0.34	0.3
15	0.34	0.34	0.3
16	0.34	0.33	2.4
17	0.34	0.35	3.8
18	0.34	0.37	7.9

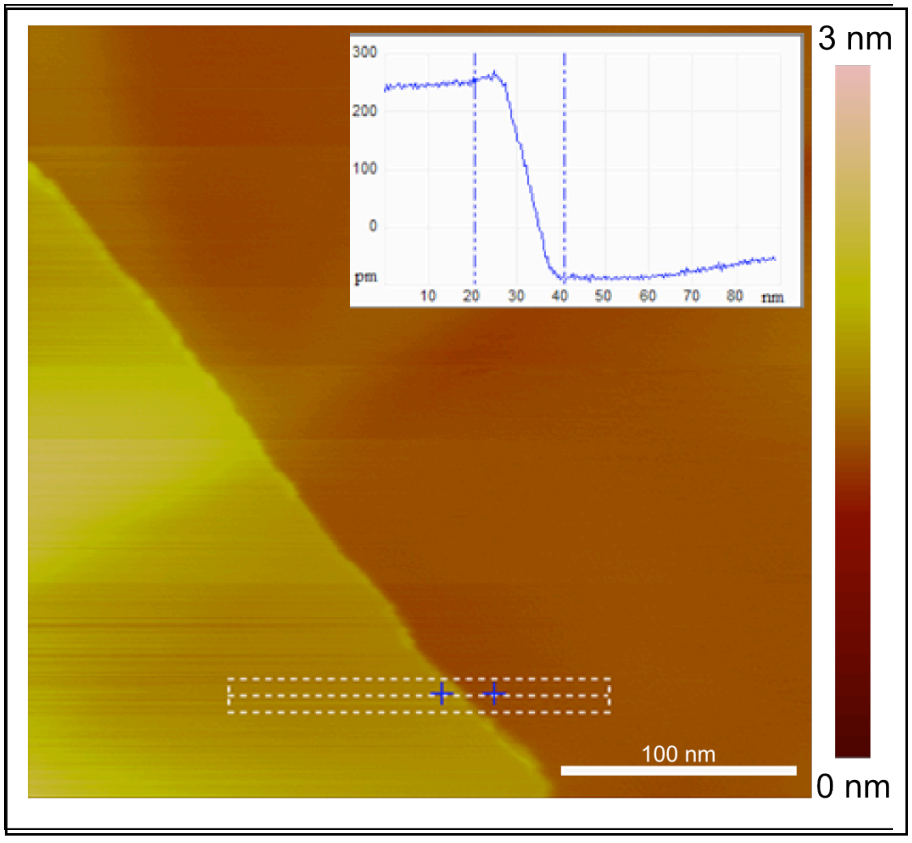

FIGURE S2. AFM height image of an atomic step on HOPG used for calibration. The profile averaging box corresponds to the inset height profile.

SUPPORTING INFORMATION S5: *AFM Height Profiles*

According to X-ray analysis, dehydrated streptavidin crystals are 4.6 nm thick.[48-51] In comparison, hydrated self-assembled monolayers (SAMs) of biotin-bound streptavidin are ~4.5 nm using Mach-Zehnder interferometry and surface plasmon techniques.[51] Although nearly identical, optical techniques often underestimate monolayer thickness by assuming a refractive index of n = 1.45 for streptavidin in air and solvent.[51] With waveguide mode spectroscopy, Busse et al., independently measured the index of refraction and the geometric thickness of phosphate buffered saline (PBS) hydrated streptavidin to be 1.42 and 8 nm, respectively.[51] Adopting these values, the experimental film thickness was ~6 nm.[51] To mitigate discrepancy between optical techniques, AFM was also performed in PBS solution.[51] AFM height data indicated that streptavidin formed a closed packed film with a sphere diameter and monolayer height of 10 nm and ~6 nm, respectively. Although comparable to waveguide mode spectroscopy, an increase in the normal stylus force during AFM imaging is known to cause a measurable decrease in the height profile of soft biological samples.[41]

Reduced AFM height profiles for soft biological samples have been corroborated by multiple studies.[41, 46-47] According to the theoretical calculations by Persson, globular proteins, such as streptavidin, will deform for forces >10 pN.[45] Experimentally, Weisenhorn et al. imaged streptavidin under different AFM contact forces and demonstrated that the maximum height varied between 1.12, 0.65, and 0.25 nm at 30, 60, and 150 pN, respectively.[44] As a consequence, the compressibility of streptavidin, in the vertical direction, was approximated to be 0.2 nm/MPa.[44]

Within this study, the mean height of free streptavidin dispersed onto freshly-cleaved mica was measured under various imaging conditions. In Fig. S3, the AFM free air drive amplitude and setpoint were modulated between 0.5 V (setpoint = 0.35V) and 2 V (setpoint = 1.75V) for a similar scan area. During sequential images under these conditions, the mean height for 10 streptavidin molecules alternated between (a) 1.3 ± 0.3 nm, (b) 0.5 ± 0.2 nm, and (c) 1.3 ± 0.3 nm, respectively. Elastic recovery of the mean streptavidin height indicates the lack of significant sample degradation.

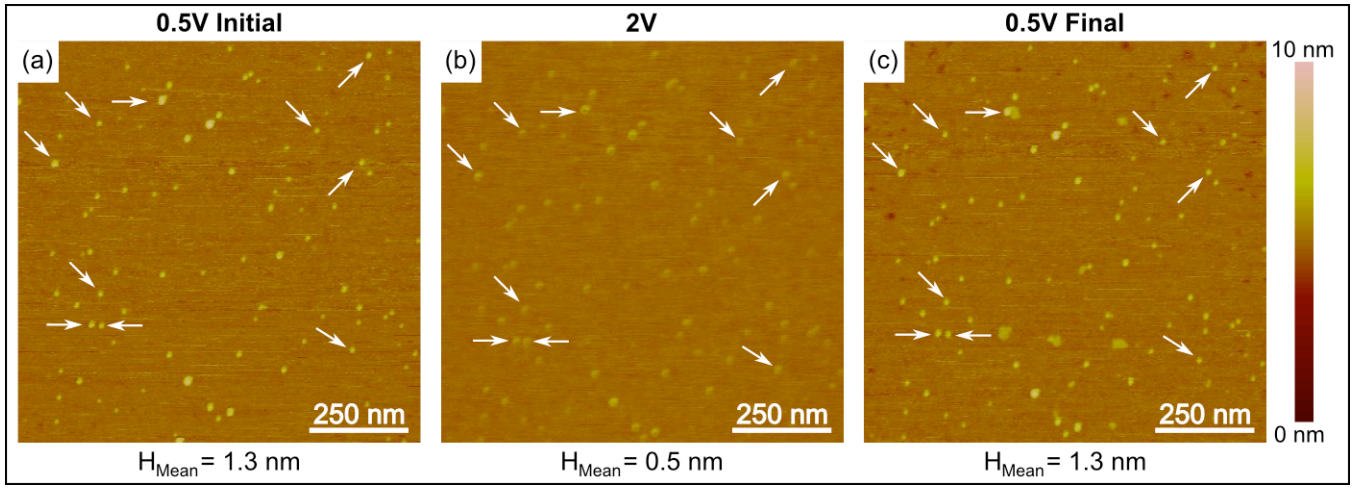

FIGURE S3. AFM images of free streptavidin dispersed onto freshly-cleaved mica. The images were acquired in succession with drive amplitudes and setpoints of (a) 0.5 V and 0.35 V, (b) 2 V and 1.75 V, and (c) 0.5 V and 0.35 V, respectively.

Further characterization of height variations under different AFM imaging conditions is provided in Fig. S4 for (a-d) bare nanotubes, (e-h) free streptavidin, and (i-l) free streptavidin-conjugated quantum dots on freshly cleaved mica. Images of the same sample area were obtained with free air drive amplitudes of 0.5 V and 2 V using setpoints at ~90% and ~50% of the drive amplitude, as shown in the traces provided below each image. The red, blue, and green traces in Fig. S4 represent the Z-piezo extending towards the surface, retracting from the surface, and setpoint, respectively. The mean heights of the features indicated by arrows are provided in the images, confirming apparent height variations under different imaging conditions. Both the nanotubes and streptavidin show decreasing heights for increased imaging forces, while the quantum dot heights are roughly constant. These results are consistent with what one would expect for AFM imaging of soft and hard materials.

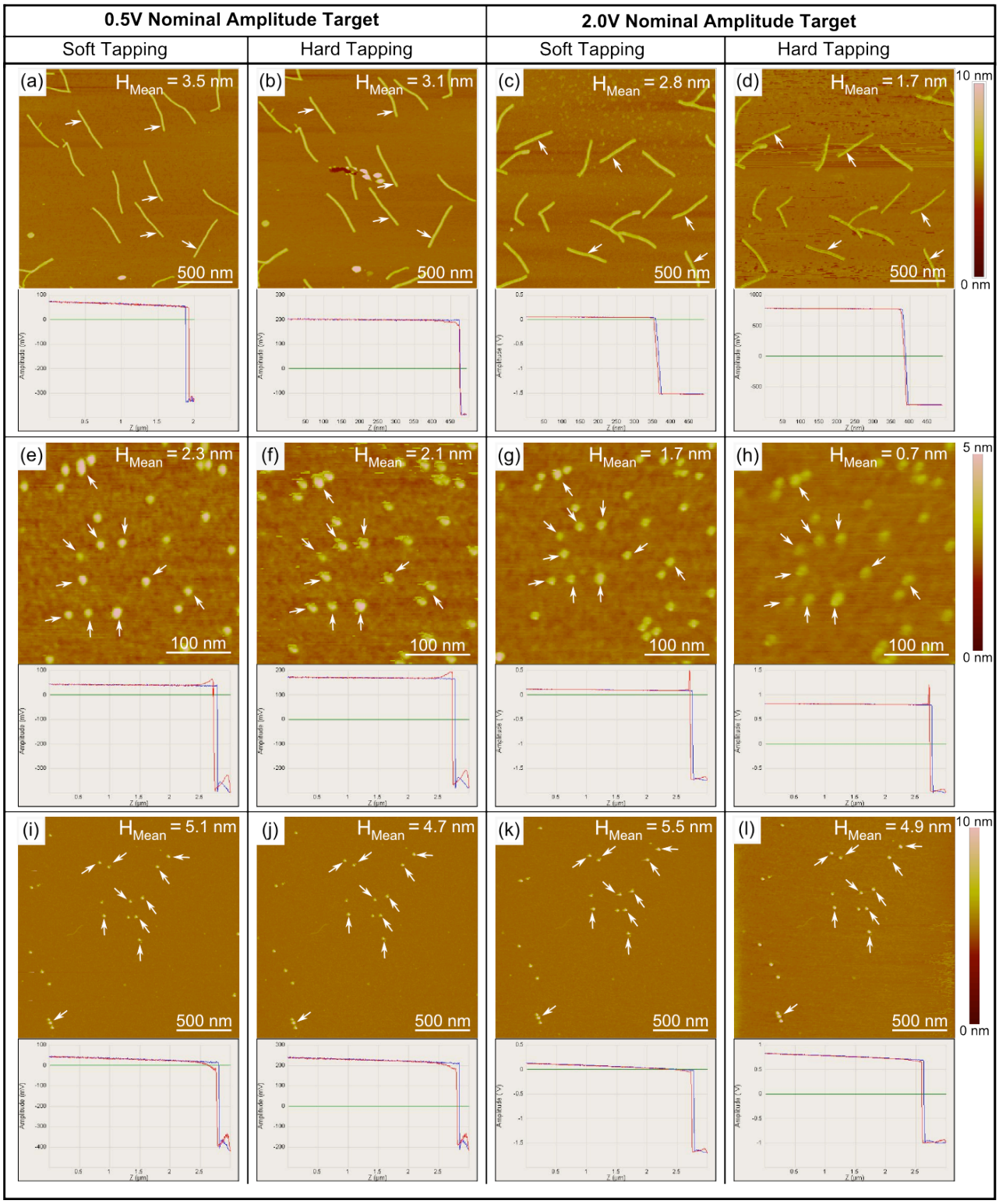

FIGURE S4. AFM height images obtained under soft and hard imaging conditions for (a-d) bare nanotubes, (e-h) free streptavidin, and (i-l) free streptavidin-conjugated quantum dots on mica. Images of the same sample area were obtained with free air drive amplitudes of 0.5 V and 2 V using setpoints at ~90% and ~50% of the free air drive amplitude, as shown in the traces provided above each image. The mean heights of the features are provided in each AFM height image.

SUPPORTING INFORMATION S6: *AFM Axial Profiles*

Axial profiles of DNA nanotubes were obtained using a box profile tool that averages height data perpendicular to the box axis. This method provides smoother height features, but absolute height information is lost by averaging. Figure S5 illustrates use of the box profile tool along the axis of functionalized DNA nanotubes with 9 available biotin binding sites. The nanotube measured in Fig. S5(a) shows 9 attached streptavidin molecules and the nanotube in Fig. S5(c) shows 9 attached streptavidin-conjugated quantum dots. The resulting profiles shown in Figs. S5(b) and (d) clearly indicate the attached particles. The reduced height scales of the resulting profiles illustrate the effects of averaging.

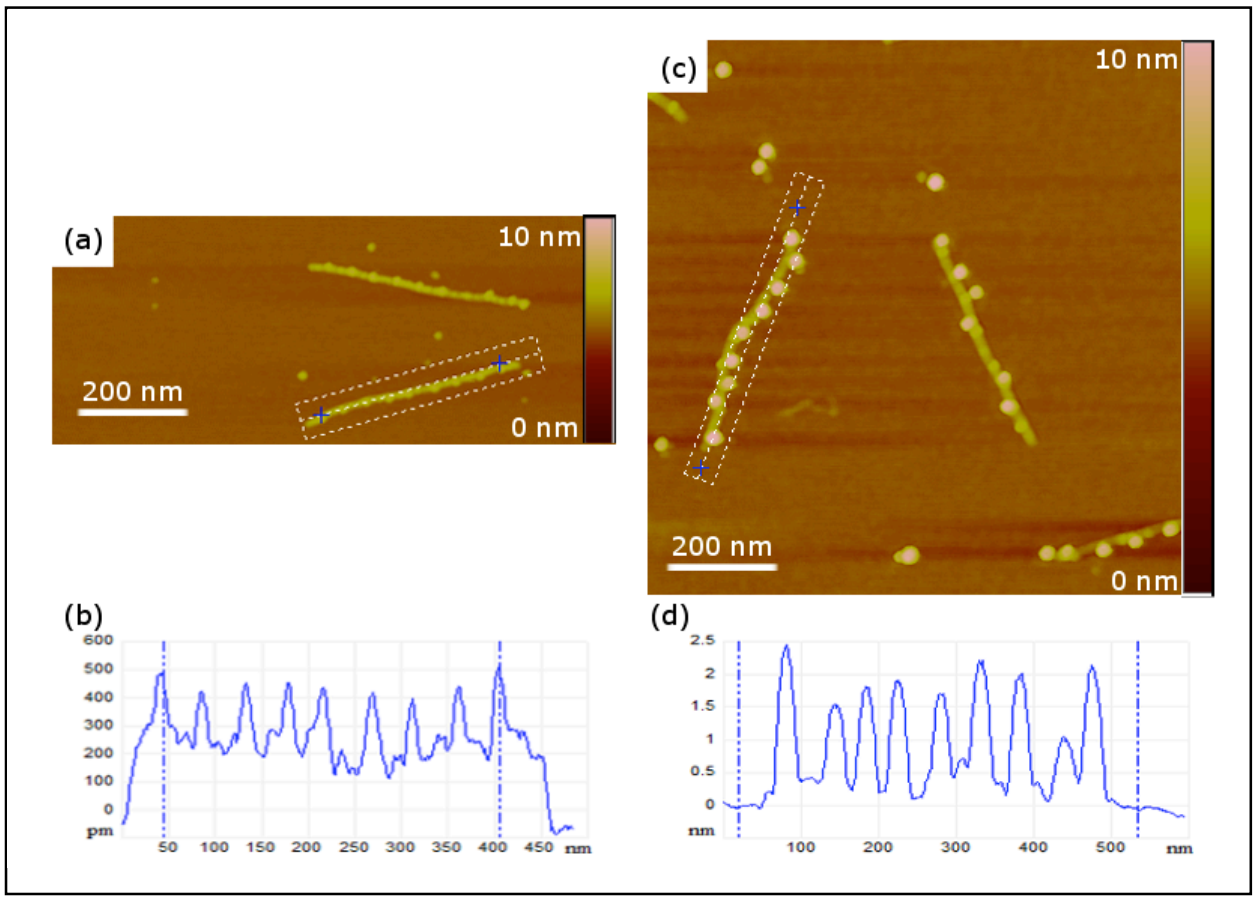

FIGURE S5. AFM height images of DNA origami nanotubes functionalized with 9 biotin binding sites showing (a) attached streptavidin and (c) attached streptavidin-conjugated quantum dots. (b) and (d) show the resulting axial profiles.

SUPPORTING INFORMATION S7: *TEM of Streptavidin-Conjugated Quantum Dots*

Transmission electron microscopy (TEM) was used to confirm the average diameter of the CdSe/ZnS core/shell quantum dots in the streptavidin-conjugated nanoparticles, as shown in Fig. S6. TEM images were obtained using a JEOL JEM-2100 HR Analytical Transmission Electron Microscope operating at 200 keV. The conjugated nanoparticles were dispersed onto an amorphous carbon coated TEM grid for imaging. The image contrast was insufficient for observing the polymer or streptavidin layers of the conjugates. Image analysis yielded an average quantum dot diameter of 5.3 ± 0.9 nm.

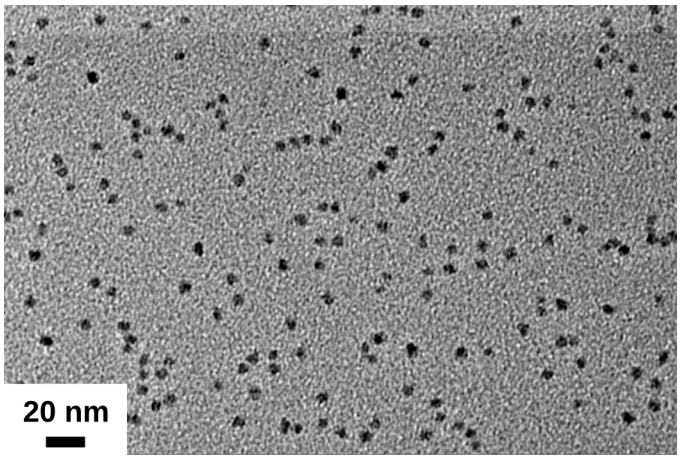

FIGURE S6. TEM image of streptavidin-conjugated quantum dots supported on an amorphous carbon thin film.

Successful attachment of quantum dots was confirmed with TEM imaging of DNA nanotubes functionalized with 29 biotin binding sites. Unstained DNA nanotubes with attached quantum dots were dispersed onto a 2 nm thick carbon film supported by a holey carbon film on a copper TEM grid. Images of the sample were acquired at 120 keV. The image shown in Fig. S7 reveals an array of 15 quantum dots formed along the length of a DNA nanotube. The average spacing of the quantum dots was 28 ± 7 nm, which agrees with the average spacing measured by AFM for nanotubes with 29 binding sites.

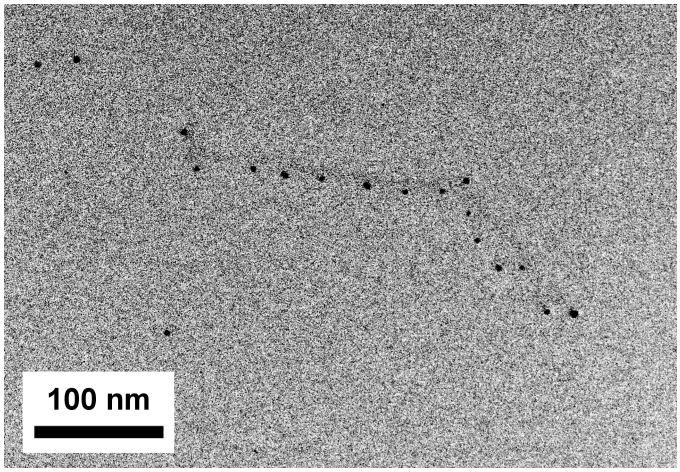

FIGURE S7. TEM image of a 15 quantum dot array formed by successful attachment to a DNA nanotube functionalized with 29 biotin binding sites. The average quantum dot spacing was 28 ± 7 nm, which agrees with the average spacing measured by AFM. The DNA nanotube was not stained, and the image was acquired at 120 keV.

SUPPORTING INFORMATION S8: *Center-to-Center Separation of Streptavidin-Conjugated QDs*

For each design periodicity, AFM images of DNA nanotubes with attached quantum dots were analyzed to measure the center-to-center separation distances between nearest-neighbor quantum dots. Histograms of the measured separations are shown in Fig. S8. In each case, no quantum dots were observed with a center-to-center separation less than 20 nm. Thus, the data indicate that in solution, the effective diameter of the streptavidin-conjugated quantum dots is 20 nm, in agreement with the specifications provided by Invitrogen.

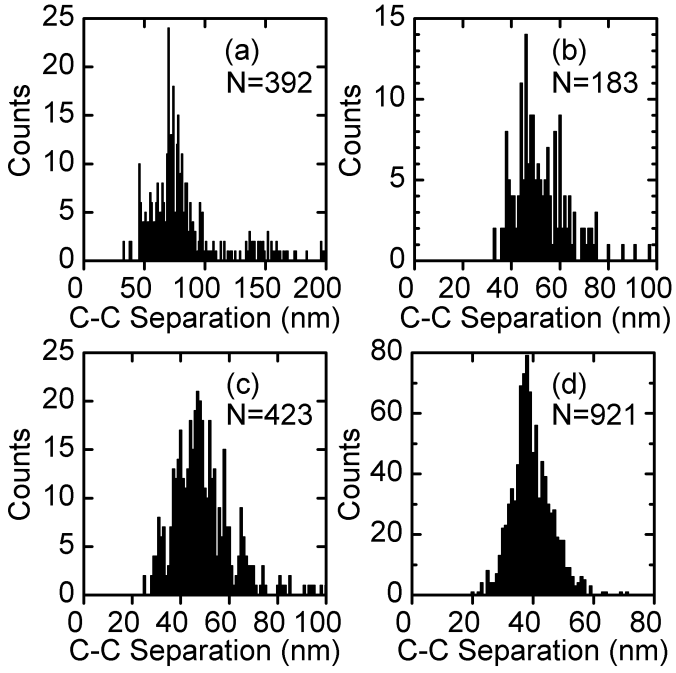

FIGURE S8. Center-to-center distance between nearest-neighbor streptavidin-conjugated quantum dots attached to DNA origami nanotubes with (a) 5, (b) 9, (c) 15, and (d) 29 biotin binding sites.

SUPPORTING INFORMATION S9: *Quantum Dot Counting Methodology*

To generate histograms of the numbers of attached quantum dots per DNA nanotube, large area AFM images of DNA nanotubes with attached quantum dots were analyzed for each designed attachment periodicity. The example AFM images in Fig. S9(a-d) illustrates the methodology used in classifying a quantum dot as attached to a DNA nanotube. Regions in which multiple nanotubes contacted each other were excluded from statistical analysis (e.g., "X" region in Fig. S9(d)). In Figs. S9(c) and (d), counted quantum dots are indicated with a circled dot. Quantum dots that appeared close to but separated from a nanotube were not counted.

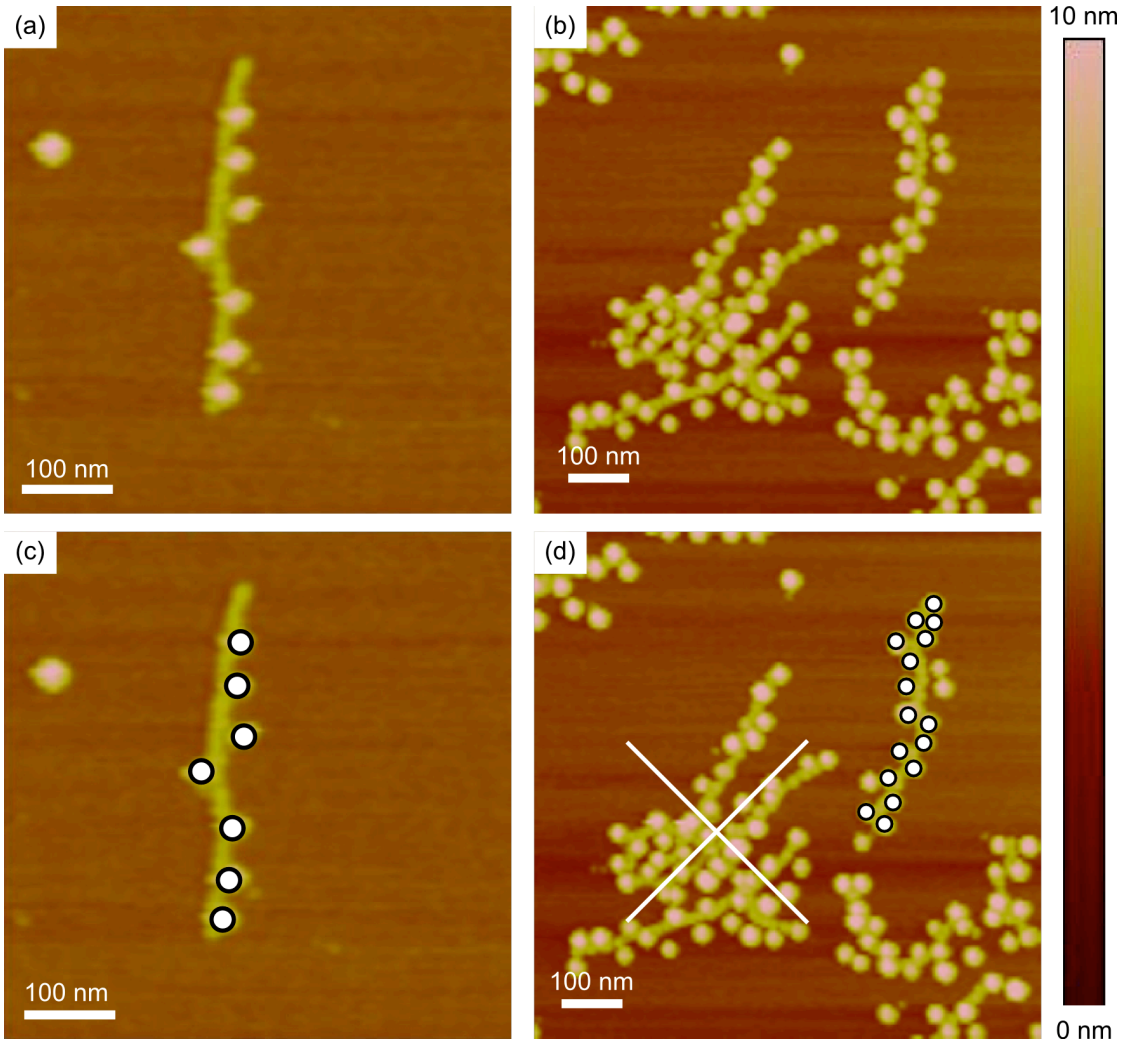

FIGURE S9. AFM height images of DNA nanotubes functionalized with (a) 9 and (b) 29 biotin sites and attached quantum dots. Images (c) and (d) illustrate counted quantum dots, while image (d) also illustrates excluded nanotubes. Counted quantum dots are marked with a circled dot.

SUPPORTING INFORMATION S10: *Attachment of Pure Streptavidin*

For the case of 5 available binding sites, AFM images of functionalized DNA nanotubes with attached pure streptavidin were analyzed to determine the number of attached molecules per nanotube. Figure S10(a) shows a histogram of the number of attached streptavidin molecules per DNA nanotube. For comparison, a histogram of the number of attached quantum dots is shown in Fig. S10(b), also for 5 available binding sites. Although the attachment histogram of streptavidin is peaked for 5 attached molecules per DNA nanotube, the average attachment probability of 0.79 for pure streptavidin attachment was calculated from Equation 2 and is only slightly higher than for quantum dot attachment. Thus, for the cases of large separations between attachment sites (no steric hindrance), the attachment probabilities for streptavidin and quantum dots may reflect missing or unavailable biotin sites.

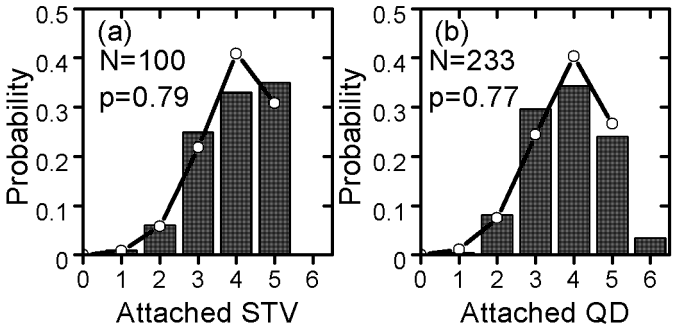

FIGURE S10. Histogram (bars) and calculated binomial distributions (lines) for the number of attached (a) pure streptavidin, and (b) quantum dots for DNA nanotubes functionalized with 5 biotin binding sites. Data for each histogram were compiled from AFM image analysis for over 100 separate nanotubes, with the exact number, N, shown in each histogram. The average attachment probabilities used to generate the binomial distributions are indicated for each case.

SUPPORTING INFORMATION S11: *Projected Nearest-Neighbor Quantum Dot Separations*

For direct evidence of steric hindrance or site poisoning, AFM images were analyzed to determine nearest-neighbor separation distances projected along the axis of the DNA nanotubes. The AFM images shown in Fig. S11 illustrate the measurement process. To facilitate accurate measurements, long white guide lines are drawn through the center of the quantum dots and perpendicular to the nanotube tangent. The projected separation is measured as the distance between the intersections of the guide lines and the nanotube axis tangents. For nanotubes with significant curvature between quantum dots, multiple axial measurements were combined, as illustrated in Fig. S11(d).

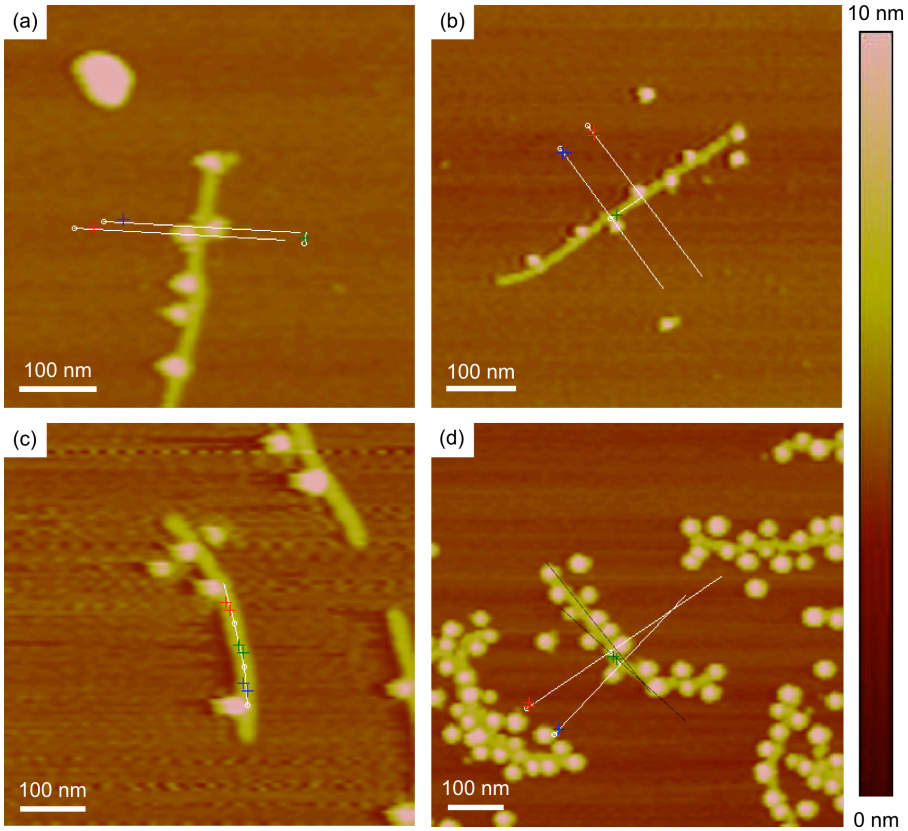

FIGURE S11. AFM images showing measurement of nearest-neighbor quantum dot separations projected along the axis of the DNA nanotube. Images (a) and (b) show the projected separation for two neighboring quantum dots whose center-to-center distances are larger than the projected separations. Image (c) and (d) show projected separation measurements for quantum dots along curved sections of the DNA nanotubes.